Transient simulations of Holocene atmospheric carbon dioxide and terrestrial carbon since the Last Glacial Maximum

Fortunat Joos,[1] Stefan Gerber,[1] I. C. Prentice,[2] Bette L. Otto-Bliesner,[3] and Paul J. Valdes[4]

Received 24 September 2003; revised 11 February 2004; accepted 18 February 2004; published 3 April 2004.

[1] Conflicting hypotheses are investigated for the observed atmospheric CO_2 increase of 20 ppm between 8 ka BP and pre-industrial time. The carbon component of the Bern Carbon Cycle Climate (Bern CC) model, which couples the Lund-Potsdam-Jena Dynamic Global Vegetation Model to an atmosphere-ocean-sediment component, is driven by climate fields from time-slice simulations of the past 21 ka with the Hadley Centre Unified Model or the NCAR Climate System Model. The entire Holocene ice core record of CO_2 is matched within a few ppm for the standard model setup, and results are broadly consistent with proxy data of atmospheric $^{13}CO_2$, mean ocean $\delta^{13}C$, and pollen data, within their uncertainties. Our analysis suggests that a range of mechanisms, including calcite compensation in response to earlier terrestrial uptake, terrestrial carbon uptake and release, SST changes, and coral reef buildup, contributed to the 20 ppm rise. The deep sea $\delta^{13}C$ record constrains the contribution of the calcite compensation mechanism to 4–10 ppm. Terrestrial carbon inventory changes related to climate and CO_2 forcing, the greening of the Sahara, peat buildup, and land use have probably influenced atmospheric CO_2 by a few ppm only. The early Holocene CO_2 decrease is quantitatively explained by terrestrial uptake and calcite compensation in response to terrestrial uptake during the glacial-interglacial transition. The recent hypothesis by *Ruddiman* [2003] that anthropogenic land use caused a 40 ppm CO_2 anomaly over the past 8 ka, preventing the climate system from entering a new glacial, would imply an anthropogenic emission of 700 GtC and a decrease in atmospheric $\delta^{13}C$ of 0.6 permil. This is not compatible with the ice core $\delta^{13}C$ record and would require an upward revision of land use emission estimates by a factor of 3 to 4. *INDEX TERMS:* 0322 Atmospheric Composition and Structure: Constituent sources and sinks; 0315 Atmospheric Composition and Structure: Biosphere/atmosphere interactions; 1615 Global Change: Biogeochemical processes (4805); 1610 Global Change: Atmosphere (0315, 0325); *KEYWORDS:* carbon cycle modeling, carbon dioxide, Holocene

Citation: Joos, F., S. Gerber, I. C. Prentice, B. L. Otto-Bliesner, and P. J. Valdes (2004), Transient simulations of Holocene atmospheric carbon dioxide and terrestrial carbon since the Last Glacial Maximum, *Global Biogeochem. Cycles*, *18*, GB2002, doi:10.1029/2003GB002156.

1. Introduction

[2] Ice core CO_2 concentration data show a decrease in atmospheric CO_2 of about 7 ppm from 11 to 8 ka before present (BP). During the later Holocene, after 8 ka BP, CO_2 increases by about 20 ppm to its pre-industrial level of ~280 ppm [*Indermühle et al.*, 1999; *Monnin et al.*, 2000; *Flückiger et al.*, 2002]. It is generally accepted that the early Holocene CO_2 decrease was caused by terrestrial carbon uptake, particularly in response to forest growth on formerly ice-covered land. The mechanisms behind the subsequent CO_2 increase are however not established.

[3] *Indermühle et al.* [1999] proposed that the main mechanism for the observed CO_2 change is terrestrial carbon uptake and release, in combination with sea surface warming and changes in the calcite cycle. They quantified the contribution of individual mechanisms by means of a double deconvolution [*Joos and Bruno*, 1998] of the ice core CO_2 record together with a limited set of ice core measurements of $^{13}CO_2$. *Indermühle et al.* [1999] estimated a terrestrial uptake of 110 gigatons of carbon (GtC) in the early Holocene followed by a release of 150 to 200 GtC

[1]Climate and Environmental Physics, Physics Institute, University of Bern, Bern, Switzerland.
[2]Department of Earth Sciences, University of Bristol, Bristol, UK.
[3]National Center for Atmospheric Research, Boulder, Colorado, USA.
[4]School of Geographical Sciences, University of Bristol, Bristol, UK.

0886-6236/04/2003GB002156$12.00

during the past 7 ka. They also implicated a sea surface warming of about 0.5°C between 9 and 6 ka BP that contributed to the observed CO_2 increase.

[4] In contrast, *Broecker et al.* [2001] suggested that the CO_2 rise after 8 ka BP was caused by marine-sediment compensation of the terrestrial carbon uptake during the early Holocene. This mechanism works as follow. First, terrestrial carbon uptake causes the concentration of carbonate ions ($[CO_3^{2-}]$) in the ocean to increase, as terrestrial uptake depletes, through gas exchange, the oceanic content of dissolved inorganic carbon (DIC: [CO2] + $[HCO_3^-]$ + $[CO_3^{2-}]$, whereas total ocean alkalinity (carbonate alkalinity: $[HCO_3^-]$ + 2 $[CO_3^{2-}]$) remains unaffected. Second, the perturbation in CO_3^{2-} (and DIC) is transported to the deep, leading to a deeper saturation horizon of $CaCO_3$ [*Broecker and Peng*, 1987] and thus to enhanced calcite sedimentation. Under these conditions, the supply of $CaCO_3$ by weathering is temporarily smaller than the loss by sedimentation, causing a decrease of the carbonate ion concentration in the ocean and an increase in ocean partial pressure of CO_2 and in atmospheric CO_2, until a new equilibrium is reached. The estimated timescale for this $CaCO_3$ compensation mechanism is of the order of 5000 years [*Broecker and Peng*, 1987; *Keir*, 1988; *Sundquist*, 1990; *Archer et al.*, 1997], as the exchange between ocean water and sediment pore water is slow. Not only compensation of terrestrial uptake during the early Holocene, as postulated by Broecker, but also of earlier uptake during the last glacial-interglacial transition (17 to 11 ka BP), as suggested by model results [*Kaplan et al.*, 2002], could have contributed to the Holocene CO_2 rise.

[5] The response of the atmosphere-ocean-sediment system to a pulse-like terrestrial uptake of 100 GtC is illustrated in Figure 1. The ocean responds to the lowered atmospheric partial pressure by releasing carbon until a new equilibrium is reached. The oceanic uptake occurs fast at the beginning and then takes centuries to equilibrate the deep oceanic water masses (left panel in Figure 1). Sediment compensation comes into play on a longer, millennial timescale and is responsible for a slow continuation of the increasing trend in atmospheric CO_2. It is this slow increase shown in the right panel of Figure 1 that emerges as a Holocene CO_2 increase according to the sediment compensation hypothesis. The impact on atmospheric CO_2 of the postulated terrestrial uptake during the deglaciation, corresponding to the first phase of the response curve, is masked by oceanic processes that forced atmospheric CO_2 to increase over the glacial-interglacial transition.

[6] Other hypotheses were formulated more recently. *Ruddiman* [2003] postulates a large release of carbon (and methane) by anthropogenic land use prior to industrialization. He argues, based on the low-resolution Vostok CO_2 data for previous glacial-interglacial cycles, that atmospheric CO_2 would have dropped naturally by 20 ppm during the Holocene and a new glacial would have started if human activities would not have caused a terrestrial carbon release during the Holocene. On the other hand, *Ridgwell et al.* [2003] suggested that coral reef buildup during the last 8 ka could explain the atmospheric CO_2 increase. Potentially, many other mechanisms, such as changes in ocean circulation and stratification, or changes in the marine biological cycle, could have affected atmospheric CO_2 during the Holocene [*Archer et al.*, 2000; *Matsumoto et al.*, 2002]. However, they lack any evidence in the Holocene proxy records.

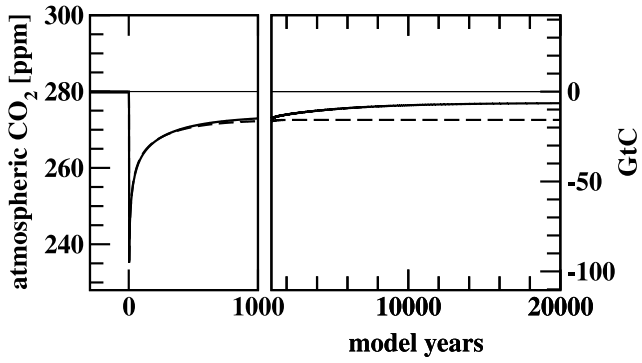

Figure 1. Response in atmospheric CO_2 of the ocean-atmosphere-sediment system to a pulse-like terrestrial uptake of 100 GtC at year 0 as simulated with the standard model setup (solid line). The left panel shows that about 85% of the initial atmospheric perturbation is removed within about 1000 years; then the ocean and atmosphere have roughly reached a new chemical equilibrium (dashed line). Ocean-sediment interaction, governed by a multi-millennial timescale, further reduces the initial CO_2 perturbation. It is the resulting slow rise in atmospheric CO_2 shown on the right panel that emerges as an atmospheric CO_2 increase according to the $CaCO_3$ sediment compensation hypothesis. The response of the atmosphere-ocean system, excluding ocean-sediment interaction in our model, is shown for comparison (dashed line). Note different *x*-axis scales for the left and right panel.

[7] A range of proxy data has the potential to provide constraints on the proposed mechanisms, but the present situation is unclear. Atmospheric $^{13}CO_2$ is affected differently by terrestrial carbon uptake in the early Holocene, release in the late Holocene, coral reef growth, or sea surface temperature changes. Unfortunately, the currently available $^{13}CO_2$ ice core data [*Indermühle et al.*, 1999] are too uncertain to firmly support or reject the different hypotheses, except the land use hypothesis of *Ruddiman* [2003]. For this hypothesis, we find a much larger than observed decrease in atmospheric $^{13}CO_2$.

[8] The relatively few records of calcite preservation in marine sediments suggest a decrease in the deep ocean carbonate ion concentration during the Holocene in qualitative agreement with the terrestrial and coral reef scenarios [*Broecker and Clark*, 2003]. However, these records do not allow to distinguish between the proposed terrestrial scenarios and the coral reef growth scenarios as each of these scenarios implies a decrease in the deep ocean carbonate concentration during the Holocene.

[9] A mass balance calculation based on $\delta^{13}C$ measurements on the calcite shells of benthic foraminifera is the most widely accepted data-based method to reconstruct terrestrial carbon inventory changes over glacial-intergla-

cial periods. This method yields a terrestrial biosphere carbon inventory that is reduced by about 300–700 GtC [*Shackleton*, 1977; *Duplessy et al.*, 1988; *Curry et al.*, 1988; *Bird et al.*, 1994, 1996] at the Last Glacial Maximum (LGM), about 21 ka BP, compared to pre-industrial time. This is a constraint on the overall terrestrial uptake during the last glacial-interglacial transition and the early Holocene and, therefore, on the magnitude of calcite compensation.

[10] Terrestrial pollen data provide information about the biome distribution during the mid-Holocene and the Last Glacial Maximum [*Harrison et al.*, 1998; *Jolly et al.*, 1998; *Prentice et al.*, 2000]. These data can help to evaluate dynamic vegetation models used to simulate terrestrial carbon storage. Estimates of postglacial terrestrial carbon uptake based on pollen data have suggested larger values than the ^{13}C mass balance approach (range of best estimates: 700–1400 GtC) [*Adams et al.*, 1990; *Van Campo et al.*, 1993; *Crowley*, 1995; *Adams and Faure*, 1998], but these are very approximate due to large gaps in the data considered, and assumptions about the average carbon density of different biomes. For the past 8 ka, *Adams and Faure* [1998] estimated from pollen data a terrestrial uptake of 170 GtC, in direct contradiction to the terrestrial release postulated by *Indermühle et al.* [1999] and *Ruddiman* [2003].

[11] Mechanistic modeling studies have addressed Holocene atmospheric CO_2 variations. *Brovkin et al.* [2002] have performed transient simulations over the past 8 ka, forcing their earth system model with orbital variations. They simulated a terrestrial carbon release of 90 GtC, qualitatively in line with *Indermühle et al.* [1999], and they were able to match the ice core CO_2 record by prescribing an additional calcite accumulation in sediments of 270 GtC. *Ridgwell et al.* [2003] forced a multibox ocean model that includes a sediment module with off-line calculated terrestrial carbon emissions [*Kaplan et al.*, 2002] and a coral reef buildup scenario over the past 21 kyrs. They found that coral reef buildup could explain a late Holocene atmospheric CO_2 rise of up to 40 ppm.

[12] Here we present results of transient simulations over the past 21 ka. A fast atmosphere-ocean-sediment-land biosphere carbon cycle model [*Joos et al.*, 2001] is forced with climate fields obtained from time-slice simulations with two ocean-atmosphere general circulation models. The modest CPU requirements of the model allowed us to perform transient sensitivity simulations to explore uncertainties in input climate fields, and to quantify the importance of different carbon-cycle processes for the changes in atmospheric CO_2 over the Holocene. The focus is on changes in the terrestrial system and on the calcite compensation mechanism, whereas coral reef buildup and other sediment-ocean interaction processes are not addressed.

[13] Models and methods are described in the next section. Then we begin our analysis with simulations of terrestrial carbon stock changes over the past 21 kyr (section 3.1) before addressing atmospheric CO_2 variations over the Holocene (section 3.2). In the following subsections, model results for atmospheric $^{13}CO_2$ (section 3.3), mean ocean $\delta^{13}C$ (section 3.4), and biome distributions (section 3.5) are compared with proxy records. The land use scenario by *Ruddiman* [2003] is discussed in section 4.

2. Models and Methods

2.1. Model Components

[14] The carbon cycle model includes the Lund-Potsdam-Jena Dynamic Global Vegetation Model (LPJ-DGVM) [*Sitch et al.*, 2003], an impulse response function (IRF) substitute of the HILDA ocean model [*Siegenthaler and Joos*, 1992; *Joos et al.*, 1996] and a well-mixed atmosphere, as in earlier studies [*Joos et al.*, 2001; *Gerber et al.*, 2003]. The equations for ocean carbonate chemistry were adjusted to extend their validity to low CO_2 concentrations. An IRF formulation for ocean-sediment interaction was added, based on the work of *Archer et al.* [1997], to account for the $CaCO_3$ compensation mechanism operating on glacial-interglacial timescales. The model and its component have been extensively tested in other contexts [*Joos et al.*, 1991, 1997; *Joos and Bruno*, 1998; *Sitch*, 2000; *McGuire et al.*, 2001; *Dargaville et al.*, 2002].

[15] The LPJ-DGVM simulates photosynthesis, respiration, fire, and the growth and competition of nine plant functional types (PFT). PFT distributions are constrained by bioclimatic limits for plant survival and regeneration, while the relative performance of PFTs, in competition for light and water, is governed by PFT-specific physiological, phenological, growth, and disturbance-response parameters. The uptake of ^{13}C is calculated following *Scholze et al.* [2003] based on work by *Lloyd and Farquhar* [1994] and *Kaplan and Prentice* [2002]. The model is driven by atmospheric CO_2 and monthly fields of temperature, precipitation, and cloud cover. The spatial resolution is set here to $3.75° \times 2.5°$.

[16] The IRF substitute of the HILDA model yields identical results to HILDA, and is used here for computational efficiency. Surface-to-deep tracer transport is described by an IRF. The nonlinearities in air-sea gas exchange and carbonate chemistry are captured by separate equations. The effect of sea surface temperature (SST) variations on carbonate chemistry is included [*Joos et al.*, 1999], whereas the impacts of changes in ocean circulation and in the marine biological cycle on atmospheric CO_2 are neglected. The parameterization of the chemistry of dissolved inorganic carbon [*Joos et al.*, 2001] used in earlier studies has been replaced. Carbonate chemistry and oceanic partial pressure of CO_2 are instead calculated from explicit carbon chemistry equilibrium equations using the solubility coefficient and dissociation constants based on work by *Weiss* [1974] and *Goyet and Poisson* [1989], because the parameterization given by *Joos et al.* [2001] has been validated only for a limited range of CO_2 concentrations. Tests revealed, however, that the two methods yield nearly identical results.

[17] $CaCO_3$ sedimentation is calculated based on an IRF as described in Appendix A. In the standard formulation, 70% of terrestrial carbon uptake is compensated on a e-folding timescale of 5000 years (Figure 1). In sensitivity experiments, the timescale was varied or the IRF was

calculated using three timescales and coefficients and their uncertainties as suggested by *Archer et al.* [1997]. The IRF approach is capturing the response of a 3-D ocean-sediment model for the calcite compensation of a carbon removal (addition) from (into) the atmosphere-ocean-sediment system, while using much less computational power than an explicit model. However, the IRF approach as used here is not adequate to address coral reef buildup or other changes in the ocean-sediment system.

2.2. Climate Boundary Conditions

[18] Changes in precipitation and temperature for the last 21 ka were derived from time-slice simulations with two climate models, the Hadley Centre Unified Model (UM) [*Pope et al.*, 2000; *Hewitt et al.*, 2001] and the NCAR Community Climate Model 1.4—paleo version (CSM) [*Boville and Gent*, 1998; *Otto-Bliesner and Brady*, 2001; *Shin et al.*, 2002; *Liu et al.*, 2003].

[19] The UM consists of the HadSM3 atmospheric circulation model [*Pope et al.*, 2000] coupled to a slab ocean model and a sea-ice model as described by *Hewitt et al.* [2001]. The atmosphere has a resolution of $2.5° \times 3.5°$, with 19 vertical layers. The climate fields used here consist of 19 snapshots carried out roughly every 1000 years up to pre-industrial time. At every time-slice, the model is driven by orbital forcing, observed atmospheric CO_2, and methane concentration. Ice sheet distribution and sea level is prescribed following *Peltier* [1994] until 7 ka BP and for present conditions thereafter. Land surface conditions were varied, by coupling the model asynchronously with the BIOME4 equilibrium vegetation model [*Kaplan et al.*, 2002]. The ocean heat flux convergence was held in all simulations at present-day values.

[20] The NCAR paleo-CSM [*Boville and Gent*, 1998] consists of a coupled atmosphere and ocean general circulation, a dynamic sea-ice model, and a land-surface biophysics model. It has a spectral resolution of T31 for the atmosphere and land-surface and a spatially variable 3-D grid for the ocean and the sea-ice components [*Otto-Bliesner and Brady*, 2001]. One simulation was done with boundary conditions for 21 ka BP [*Shin et al.*, 2002] (sea level, ice sheet distributions, and low greenhouse gas concentrations). Further simulations were performed over the course of the Holocene at 11, 8.5, 6, 3.5, and 0 ka (pre-industrial) BP [*Liu et al.*, 2003]. Only the orbital parameters were varied in these Holocene simulations. Hence the two simulations in the early Holocene must be interpreted with caution as ice sheet extent was considerably different at 11 ka and 8 ka BP compared to present conditions. Carbon cycle model results obtained with CSM climate output are disregarded for the first half of the Holocene (10.5 to 6 ka BP). Although the model set-up is not ideal for the early Holocene, simulations with the CSM climate fields allow an independent check on various results obtained with the UM climate fields as the typical memory of the ocean-atmosphere-terrestrial system is 1 ka or less and the exact evolution of terrestrial carbon inventory variations is not crucial for the overall magnitude of the calcite compensation mechanism (see section 3.2).

[21] For the LGM, simulated global mean temperature is approximately 4°C lower and global mean SST about 2°C lower than today in both models (Figure 2). The models also yield comparable changes in land temperature for different latitude bands between the LGM and today. The relative high temperatures simulated with the CSM at 11 and 8.5 ka BP are probably influenced by the unrealistic assumption of a present-day ice sheet boundary. Precipitation simulated with the two climate models is comparable on a global scale for the LGM. The CSM yields a more pronounced reduction in precipitation over land areas between 30°N and 90°N than the UM. In the late Holocene, both models show a decreasing trend in precipitation over land.

[22] The monthly temperature, precipitation, and cloud-cover fields applied to force the LPJ-DGVM were obtained by summing (1) monthly mean deviations from the pre-industrial state, (2) a monthly climatology based on observations and (3) monthly interannual anomalies. First, the monthly values of each time-slice were averaged over the length of the simulation to obtain monthly means. Then, the time-averaged monthly values of the pre-industrial reference simulation were subtracted from those of each time-slice. The resulting monthly mean climate deviations were linearly interpolated in time between the midpoints of the time slices to obtain continuous records for the period from 21 ka BP to present for both the UM and the CSM model. Second, the monthly values of a present-day mean climatology [*Leemans and Cramer*, 1991; *Cramer et al.*, 2001] were added to the monthly mean deviations. Third, interannual anomalies were determined for individual months by detrending observational data [*New et al.*, 2000] for simulations with the UM climate fields or from the first 50 years of the pre-industrial run for simulations with the CSM fields. Then, the interannual anomalies were added repeatedly over the 21 ka period. Cloud-cover data for the CSM simulations were not available. The pre-industrial cloud fields as derived from the UM model output were therefore used in all simulations with CSM temperature and precipitation fields. The deviations in global mean SST used to force the HILDA ocean model were calculated from the mean deviations of each time slice with respect to the pre-industrial global mean SST. Climate and SST variations at multidecadal or centennial timescales such as the Younger Dryas or the 8.2 ka BP event are implicitly neglected. Similarly, changes in interannual variability, as far as not captured in the averaged anomaly fields, are neglected, but changes in the seasonality as simulated by the climate models over the past 21 ka are taken into account. Interannual variability is a necessary driver for the model's fire module, but magnitude and timing of fire fluxes depend on the amount of material available for burning and the neglect of changes in interannual variability is not considered as critical for this application.

[23] The ice sheet and ocean-land mask of the UM was used to identify areas suitable for plant growth. During the deglaciation, this area increased by 7.7×10^{12} m^2 (Figure 3). The loss of land by sea level increase was outweighed by the gain of land from ice sheet retreat. The carbon stored on a grid cell that becomes flooded due to sea level rise is assumed to enter the atmosphere with an e-folding timescale

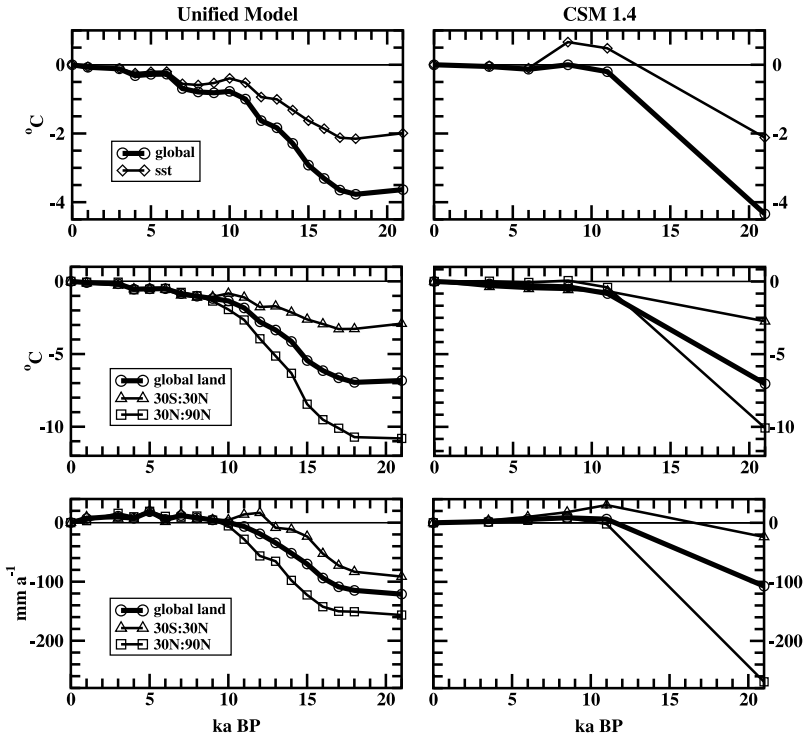

Figure 2. Temperature and precipitation anomalies from time slice simulations with the Hadley Centre UM and the NCAR CSM. Changes are given as mean deviation relative to the pre-industrial control simulation. The symbols represent individual time slice simulations. (top) Global averaged surface and sea surface temperature. (middle) Surface temperature over land. Global averages, excluding Antarctica, and averages for the latitudinal bands between 30°S and 30°N, and between 30°N and 90°N, are shown. (bottom) Changes in precipitation over land, global, and for two latitudinal bands.

of 100 years. Sensitivity experiments have shown that the long-term evolution of atmospheric CO_2 is not affected, whether terrestrial carbon stored initially on a submerged grid cell is released to the atmosphere immediately or gradually.

2.3. Spin-Up, Atmospheric CO_2, and Transient Simulations

[24] The LPJ-DGVM is spun up from bare ground for 1000 years under glacial conditions, i.e., the climate fields for 21 ka BP and atmospheric CO_2 of 186 ppm. Soil carbon stock was calculated based on litter input and mean decomposition rate after 400 years in order to reduce the time required to approach equilibrium. The IRF ocean substitute does not require a spin-up. Total carbon storage is 2100 GtC at the LGM.

[25] Two types of transient simulations were performed. In the set of experiments presented in sections 3.1, atmospheric CO_2 was prescribed during the last deglaciation and the Holocene according to ice core data [*Monnin et al.*, 2000; *Flückiger et al.*, 2002] in order to investigate changes in terrestrial carbon storage and vegetation distribution under realistic CO_2 forcing. In a second set of experiments presented in section 3.2, the evolution of atmospheric CO_2 during the Holocene is modeled and the mechanisms responsible for the simulated Holocene CO_2 variations are quantified. Again, atmospheric CO_2 is prescribed during the

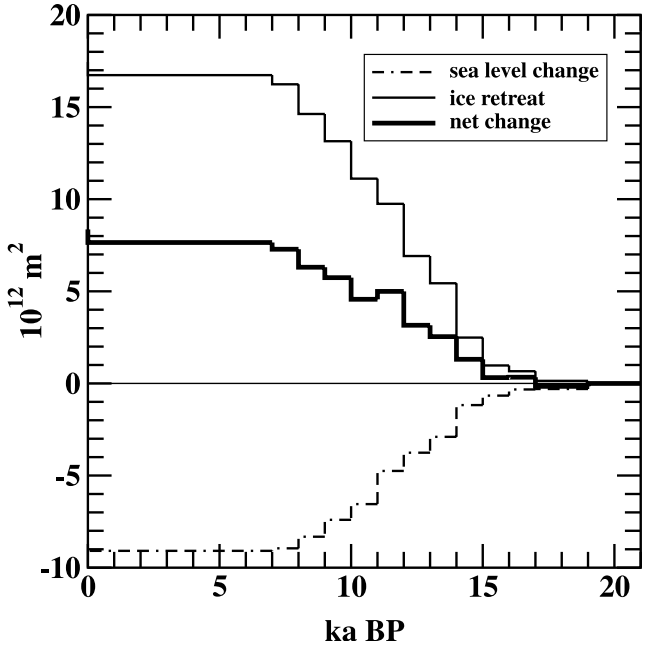

Figure 3. Changes in land available for plant growth relative to 21 ka BP in response to ice sheet retreat (thin solid line) and sea level rise (dash-dotted line) and the resulting net change (thick solid line).

Table 1. Model Setup and Boundary Conditions for the Various Simulations[a]

Simulation	T, ka BP	Model Setup
		Atmospheric CO_2 Prescribed From LGM (21 ka BP) Until Pre-Industrial Time (0 ka BP)
P1; P1-CSM		atmospheric CO_2 from Dome C ice core
P2; P2-CSM		atmospheric CO_2 set constant to 280 ppm
		Atmospheric CO_2 Simulated During the Holocene[b]
S1	10.5	standard simulation
S2; S2-CSM	8.0	$CaCO_3$ compensation only (timescale: 5 ka), SST and terrestrial carbon inventory kept constant after *T*
S2a; S2a-CSM	8.0	$CaCO_3$ compensation only (timescales varied between 1 and 50 ka)
S2b; S2b-CSM	8.0	$CaCO_3$ compensation only (multiple timescales)
S3	8.0	$CaCO_3$ compensation and SST, terrestrial carbon inventory kept constant after *T*
S4	10.5	CO_2 fertilization shut off during the whole simulation
S5	10.5	CO_2 fertilization shut off after *T*
S6	10.5	no changes in ice sheet ocean land mask after *T*

[a]Simulations, where the CSM climate fields were applied are labeled "CSM"; otherwise the UM climate fields were used.
[b]Start of simulation at LGM; atmospheric CO_2 is prescribed until T and simulated thereafter.

last deglaciation, as we are not in a position to model the CO_2 variations during the deglaciation with our model setup. A summary of the various experiments is provided in Table 1.

3. Results

3.1. Changes in Terrestrial Carbon Stock

[26] We start our discussion by analyzing the simulated evolution of terrestrial carbon storage over the past 21 kyr. The multimillennia timescales governing calcite compensation imply that the amount and timing of terrestrial carbon uptake during the glacial-interglacial transition and the Holocene must be estimated to quantify the overall effect of terrestrial stock changes on Holocene CO_2 variations.

[27] In Table 2 the simulated changes in terrestrial carbon inventory and the contribution of different forcing factors and regions to these changes are summarized for selected periods. The LPJ-DGVM was forced by changes in climate and atmospheric CO_2 in simulations P1 and P1-CSM, whereas atmospheric CO_2 was held constant at the pre-industrial value of 282 ppm in the simulations P2 and P2-CSM. Thus simulation P2 (P2-CSM) shows the effect of climate change on terrestrial storage. The difference between P1 and P2 (P1-CSM minus P2-CSM) is due to CO_2 fertilization. Differences in global terrestrial stock changes between simulations with the UM and the CSM climate

Table 2. Factorial Analysis of Changes in Terrestrial Carbon Inventory During the Past 21 ka[a]

		UM				CSM			
Simulation		Ice Retreat	Sea Level	Remaining Area	Total Change	Ice Retreat	Sea Level	Remaining Area	Total Change
21–11 ka BP									
P1	CO_2 and climate	352	−133	460	**679**	342	−144	367	565
P2	climate only	364	−181	−70	**113**	353	−198	−176	−21
P1–P2	CO_2 fertilization	−12	48	530	**566**	−11	54	543	586
11–8 ka BP									
P1	CO_2 and climate	139	−67	30	**102**	140	−66	53	127
P2	climate only	145	−61	21	**105**	144	−68	50	126
P1–P2	CO_2 fertilization	−6	−6	9	**−3**	−4	2	3	1
8–6 ka BP									
P1	CO_2 and climate	13	−6	4	**11**	11	−4	76	83
P2	climate only	13	−6	−36	**−29**	11	−4	46	53
P1–P2	CO_2 fertilization	0	0	40	**40**	0	0	30	30
6–0 ka BP									
P1	CO_2 and climate	0	0	28	**28**	0	0	75	**75**
P2	climate only	0	0	−88	**−88**	0	0	−25	**−25**
P1–P2	CO_2 fertilization	0	0	116	**116**	0	0	100	**100**
21–0 ka BP									
P1	CO_2 and climate	610	−193	403	**820**	603	−199	446	**850**
P2	climate only	609	−259	−249	**101**	602	−269	−200	**133**
P1–P2	CO_2 fertilization	1	66	652	**719**	1	70	646	**717**

[a]For both the UM and the CSM climate fields, simulations with variable (simulation P1, P1-CSM), and a simulation with constant atmospheric CO_2 (simulation P2, P2-CSM) have been performed. CO_2 fertilization is taken as the difference between the two simulations. The changes are distinguished for land covered by ice at the beginning of each period (Ice Retreat), land that has been flooded (Sea Level), and the remaining land, where changes in carbon inventories are driven only by changes in temperature, precipitation, cloud-cover, and atmospheric CO_2. We note that the CSM simulations at 11 and 8 ka BP consider changes in orbital forcing only, whereas otherwise present-day boundary conditions are applied; the numbers for the period 21 to 11 ka BP, 11 to 8 ka BP, and 8 to 6 ka BP must be interpreted with caution and are given here for completeness. The area affected by ice retreat and the size of the remaining area is different for the different evaluation periods, and the data shown in the columns "Ice Retreat" and "Remaining Area" are not additive over periods.

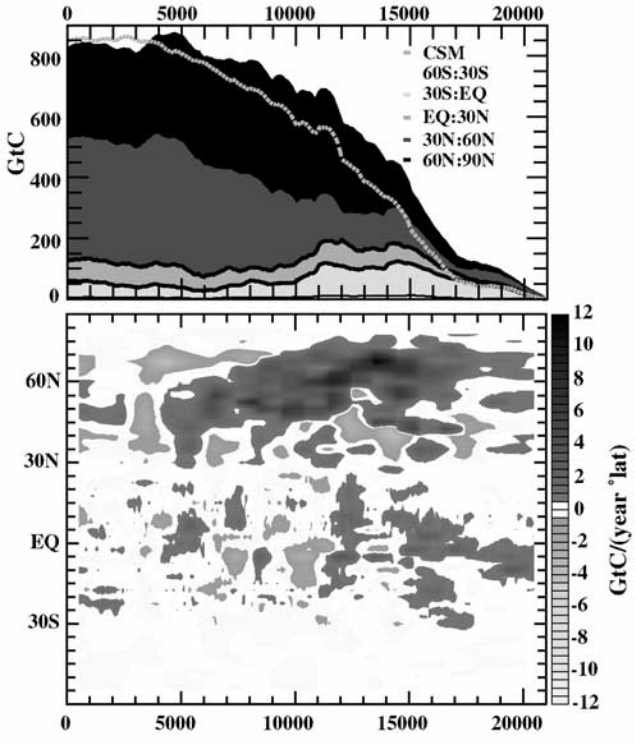

Figure 4. Simulated changes in terrestrial carbon inventory. (top) Cumulative change for different latitude bands for the UM climate anomalies (simulation P1) and global changes for the CSM climate anomalies (dotted line, simulation P1-CSM). The results have been smoothed by a 50-year running mean filter to remove high-frequency variability. (bottom) Zonally integrated net ecosystem uptake (1000-year running means) for the UM climate anomalies (simulation P1). See color version of this figure at back of this issue.

anomalies are generally surprisingly small, not only for the overall change, but also with respect to the contribution of different forcing factors during different periods.

[28] *Kaplan et al.* [2002] performed transient simulations with LPJ-DGVM applying the UM climate anomalies for the past 21 ka and the global inventory changes for simulation P1 and P2 are broadly similar to their results. Here modeled land carbon inventory changes are evaluated for formerly ice-covered areas, for areas flooded by sea level rise, and for the remaining land to quantify the impact of ice sheet retreat, sea level rise, temperature, precipitation, and cloud-cover changes on terrestrial carbon storage (Table 2).

[29] For the period from the LGM to pre-industrial time, the modeled total terrestrial uptake is 820 GtC for the UM climate anomalies (simulation P1) and 850 GtC for the CSM anomalies (P1-CSM). About 80% of the modeled LGM-pre-industrial uptake occurs between 17 ka and 11 ka BP (Figure 4) when changes in the driving variables are large. The LGM-pre-industrial change is comparable [*François et al.*, 1999; *Otto et al.*, 2002] or somewhat higher than the results obtained by others [*Esser and Lautenschlager*, 1994; *Friedlingstein et al.*, 1992; *François et al.*, 1998; *Beerling*, 1999] who have forced terrestrial carbon models with model derived LGM climate fields and atmospheric CO_2. CO_2 fertilization contributes most (~700 GtC) to the simulated total change, as also found in previous studies with biogeochemical models [*Esser and Lautenschlager*, 1994; *François et al.*, 1998, 1999; *Otto et al.*, 2002]. During the transition, CO_2 fertilization leads to a modeled terrestrial uptake of ~540 GtC in areas not affected by inundation or ice retreat. A role for CO_2 fertilization in determining terrestrial carbon storage at concentrations of CO_2 within the glacial-interglacial range (180 to 280 ppm) has support from a range of data-based studies [*Peng et al.*, 1998; *DeLucia et al.*, 1999; *Bennett and Willis*, 2000; *Cowling and Field*, 2003]. The magnitude of the CO_2 fertilization response in our model is consistent with the recent amplification of the seasonal cycle in atmospheric CO_2 [*McGuire et al.*, 2001; *Dargaville et al.*, 2002] and with the enhancement of net primary production shown in Free Air Carbon Dioxide Enrichment experiments [e.g., *DeLucia et al.*, 1999; T. Hickler, unpublished results, 2003].

[30] Climate forcing factors have a substantial impact on terrestrial storage on a regional level. However, carbon uptake in response to vegetation growth on formerly ice-covered areas is partly compensated by carbon loss due to sea level rise and due to changes in temperature and precipitation elsewhere. These compensating fluxes explain the modest contribution (100 and 130 GtC, simulations P2 and P2-CSM) from the combined climate forcings to the global carbon uptake. Vegetation growth on formerly glaciated areas leads to an uptake of more than 600 GtC for both the UM and the CSM climate anomalies, whereas sea level rise leads to a loss of ~260 GtC during the transition and the early Holocene. Changes in temperature and precipitation lead to a carbon loss of 250 and 200 GtC for the UM and the CSM anomalies, on areas not affected by sea level rise and ice sheet retreat, respectively. This loss is caused by higher turnover rates of the litter and soil pools under a warmer climate, whereas the total amount of carbon stored in vegetation on these areas remained almost constant between 21 ka and 8 ka BP. The simulated climate driven uptake is comparable to estimates of *Prentice and Fung* [1990] as revised upward by *Friedlingstein et al.* [1995] and those of *Friedlingstein et al.* [1992], who combined climate model output for the LGM and bioclimatic schemes, without considering CO_2 fertilization effects.

[31] During the past 8 ka, simulation P1 (in which both climate and CO_2 fertilization effects are included) yields a terrestrial carbon uptake of ~40 GtC. This is in contradiction to the release postulated by *Indermühle et al.* [1999], but it is bracketed amply by earlier model results that range from a terrestrial release of 90 GtC to an uptake of 370 GtC during the late Holocene [*Foley*, 1994; *François et al.*, 1999; *Beerling*, 2000; *Brovkin et al.*, 2002; *Kaplan et al.*, 2002]. CO_2 fertilization is mostly responsible for the uptake in simulation P1, whereas changes in sea level and ice sheet extent have a negligible impact. On the other hand, simu-

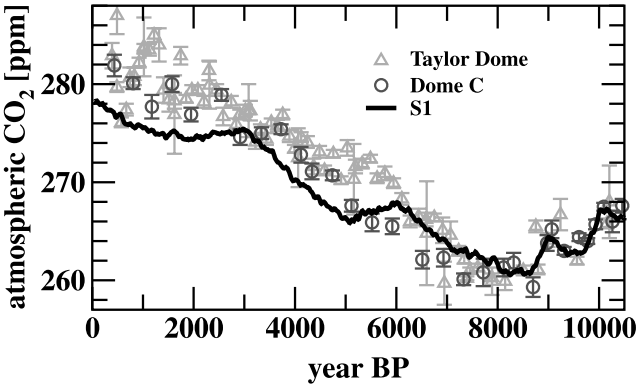

Figure 5. Simulated atmospheric CO_2 (solid line) versus the Holocene ice core CO_2 record (symbols). Model results are for the standard simulation S1 using the UM climate anomalies and have been smoothed by 50-year running means. Climate anomalies have been linearly interpolated between time-slice simulations. This results in step-like changes in the atmospheric CO_2 growth rate. Ice core data are from Dome C (circle) *Flückiger et al.* [2002] and Taylor Dome (triangle) *Indermühle et al.* [1999]. The differences in the ice core data between 7 and 5 ka BP arise from uncertainties in the age scale of the two ice cores [*Stauffer et al.*, 2002].

lation P2 (in which CO_2 fertilization is suppressed) yields a terrestrial release of ~120 GtC. A release, albeit smaller, was also obtained in simulation P2-CSM for the period 6 to 0 ka BP (recall that we are disregarding the CSM-based carbon simulations for the early Holocene). The simulated uptake of 100 GtC (Simulation P1) between 11 ka and 8 ka is mainly driven by ice sheet retreat and sea level rise and is in agreement with the atmospheric data-based estimate of 110 GtC by *Indermühle et al.* [1999].

[32] In conclusion, terrestrial carbon storage is simulated to increase over the Holocene in the standard setup (Simulations P1 and P1-CSM). Terrestrial uptake since the LGM is above the range of 300 to 700 GtC estimated from $\delta^{13}C$ mass balance calculations. We note, however, that a variety of mechanisms have been suggested which could increase this range [e.g., *Crowley*, 1991; *Spero et al.*, 1997; *Maslin and Thomas*, 2003]. On the other hand, terrestrial uptake in the climate-only simulation (P2) is below the data-based range. Hence simulations with the coupled model comparable to P1 and P2 as presented in the next section 3.2 will provide high and low estimates for the influence of sediment compensation on late Holocene CO_2.

3.2. Holocene Atmospheric CO_2

[33] The modeled Holocene evolution of atmospheric CO_2 in the standard simulation S1 matches the ice core data within a few ppm (Figure 5). The early CO_2 decrease of around 6 ppm from 10.5 to 8 ka BP is well reproduced. The relatively steep increase between 8 and 3 ka BP and the increase in the latest part of the Holocene are slightly underestimated; the simulated pre-industrial CO_2 concentration of 278 ppm is at the lower end of the observed range of ~278 to 284 ppm. Next, we present a set of sensitivity experiments to quantify the contribution of individual mechanisms to the changes simulated in S1.

3.2.1. Sediment Compensation

[34] In simulation S2, SST and terrestrial storage are kept constant after 8 ka BP. Atmospheric CO_2 then increases only by 11 ppm during the past 8 ka, much less than the observed 20 ppm increase (Figure 6). The modeled CO_2 increase of 6 ppm between 8 and 6 ka BP is comparable to that shown in the ice core data; however, the sediment compensation mechanism fails to explain the observed CO_2 increase after 6 ka BP.

[35] The sensitivity of these results to variations in the IRF of the sediment component was tested. The timescale, τ, was varied in simulations S2a over a range from 1 ka to 50 ka in steps of 1 ka (Figure 7, top). The simulated atmospheric CO_2 change for the 8 to 0 ka BP period increases from 5 ppm for τ = 1 ka, to 11 ppm for the standard model setup (τ = 5 ka), to approach a value of 14 ppm at large values of τ. Changes are slightly less when applying the CSM anomalies (simulation S2a-CSM) We also tried multiple timescales of 5.5 ka, 8.2 ka, and 200 ka (simulations S2-b) instead of a single timescale of 5000 years; the relative weights of the three timescales were varied within their uncertainties (0.4–0.6, 0.1–0.28, and 0.3–0.32) (see Appendix A). The simulated CO_2 increase was then higher by 0.3–1.1 ppm than the 11 ppm obtained with the standard sediment model setup.

[36] The rather low sensitivity of simulated CO_2 changes during the past 8 ka to the choice of the compensation timescale can be understood by analyzing the fraction, f, that is available between 8 ka BP and 0 ka BP for compensation under the assumption that the terrestrial uptake occurred at time t' (before 8 ka BP),

$$f(t',\tau) = 0.7 \times 0.15 \times \left[\exp\frac{-(8\,\mathrm{ka\,BP} - t')}{\tau} - \exp\frac{-(0\,\mathrm{ka\,BP} - t')}{\tau}\right]. \quad (1)$$

The factor 0.15 on the right-hand side arises as only ~15% of a perturbation of the atmosphere-ocean system remains airborne, while the rest is removed by the ocean. This airborne fraction increases with the background level of atmospheric CO_2 due to the nonlinear carbon chemistry [*Joos et al.*, 1996] and a value of 15% is a good approximation for the Holocene situation. A simulation with HILDA model where 100 GtC of carbon were removed from the atmosphere-ocean system yields an equilibrium airborne fraction of 15.8% for a background CO_2 level of 280 ppm as shown in Figure 1 (dashed line). The factor 0.7 represents the fraction of the perturbation in the combined ocean-atmosphere system that is available for sediment compensation; the rest of the perturbation is removed by the weathering cycle operating on a 200 ka timescale [*Archer et al.*, 1997]. We have varied τ between 1 and 40 ka and t' between 17 ka BP and 11 ka BP (Figure 7, bottom). Then the fraction available for sediment compensation during the past 8 ka is typically between 2 and 4%. This may be compared with the fraction of 2.9% simulated in the standard run (S1). These calculations suggest that

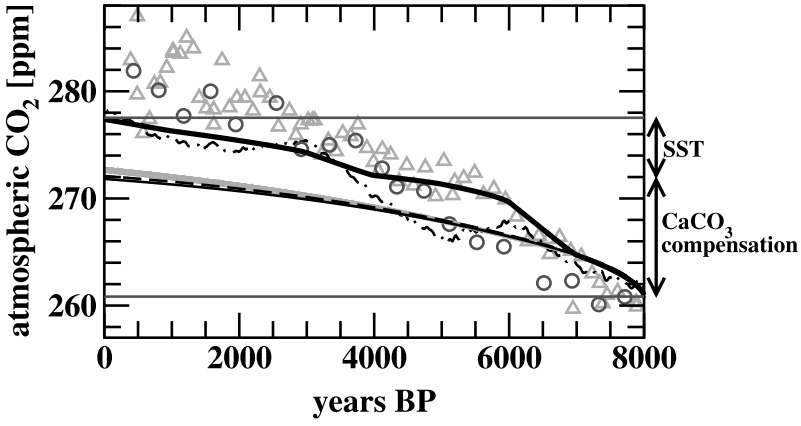

Figure 6. Contribution of the $CaCO_3$ compensation mechanism, sea surface warming, and of changes in terrestrial storage to the simulated CO_2 increase for the last 8 ka. In simulation S2 (thin solid line), only $CaCO_3$ compensation is simulated, whereas terrestrial storage and SST are kept constant after 8 ka BP. $CaCO_3$ compensation leads to a CO_2 increase of about 11 ppm during the past 8 ka. SST is also allowed to vary in simulation S3 (dash-dotted line) and atmospheric CO_2 increases by an additional 5 ppm until the pre-industrial time (difference between S3, dash-dotted line, and S2, thin solid line). The difference between the standard simulation S1 (thick solid line) and simulation S3 (dash-dotted line) is caused by changes in terrestrial carbon storage; a terrestrial uptake and subsequent release is simulated between 7 and 3 ka BP. The arrows on the right-hand side denote the contribution of the $CaCO_3$ mechanism and the effect of SST on the simulated CO_2 increase from 8 to 0 ka BP. Differences between different sediment compensation only simulations (S2, thin solid line; S2-CSM, dashed line; S2b, shaded area) are negligible as the terrestrial uptake until 8 ka is similar for the CSM and the UM anomalies, and simulated atmospheric CO_2 increase is not sensitive to the exact choice of the timescales governing sediment compensation. The CSM anomalies are applied in simulation S2-CSM (dashed line) instead of the UM anomalies (S2, thin solid line). The shaded area covers the range of results for simulations where three timescales instead of a single timescale have been used to calculate the IRF for sediment compensation and the coefficients for the IRF have been varied within their uncertainties (simulations S2b) for both the UM and the CSM climate anomalies. Ice core data are from Dome C (circle) *Flückiger et al.* [2002] and Taylor Dome (triangle) *Indermühle et al.* [1999].

uncertainties in the timescales of sediment compensation and the exact temporal evolution (as opposed to the magnitude) of terrestrial carbon uptake lead to an uncertainty of about ±30%.

[37] In summary, the CO_2 increase between 8 and 0 ka BP in response to sediment compensation is about 3% of the terrestrial uptake during the transition and the early Holocene. Uncertainties in the timescales of sediment compensation lead to an uncertainty of about ±30%. In our simulations, only slightly more than half of the observed CO_2 increase is explained by sediment compensation.

3.2.2. Sea-Surface Temperature

[38] In simulation S3, the effect of varying SST on CO_2 solubility is included as well as the $CaCO_3$ sedimentation mechanism. SST is varied according to the results from the UM model, while terrestrial carbon storage is still kept constant after 8 ka BP. The increase in SST by about 0.6°C occurs mainly between 7 and 6 ka BP and leads to an additional oceanic outgassing of about 6 ppm. Using the CSM model SST makes little difference: The difference in simulated CO_2 changes between S3-CSM and S3 over the past 6 ka is <2 ppm.

3.2.3. Terrestrial Uptake

[39] The simulated change in terrestrial storage during the past 8 ka is small. Consequently, the differences in atmospheric CO_2 between the standard simulation S1 and the simulation S3, where terrestrial storage was kept constant, are slight. The terrestrial biosphere modulates the evolution of CO_2 during the past 8 ka by taking up carbon between 6 and 5 ka, and between 3 and 2 ka BP, and releasing carbon between 5 and 3 ka, and 2 and 0 ka BP.

3.2.4. CO_2 Fertilization

[40] CO_2 fertilization on land affects the modeled evolution of Holocene atmospheric CO_2 in two opposing ways. First, CO_2 fertilization promotes a large terrestrial uptake during the deglaciation when CO_2 increased from 186 to 265 ppm. This leads to a large $CaCO_3$ compensation and thus leads to longer-term outgassing of CO_2 during the Holocene. Second, CO_2 fertilization acts as a negative feedback in the coupled land-atmosphere-ocean carbon cycle system by enhancing terrestrial uptake during times of increasing atmospheric CO_2. Thus CO_2 fertilization acts to dampen any atmospheric CO_2 increase, including increases driven by, for example, $CaCO_3$ compensation or sea-surface warming.

[41] This balance is explored by inhibiting CO_2 fertilization in simulation S4. This is done by setting the CO_2 concentration in the model's photosynthesis module to 267 ppm over the entire simulation. Simulation S4 yields a much larger decrease in CO_2 between 10.5 and 8 ka BP

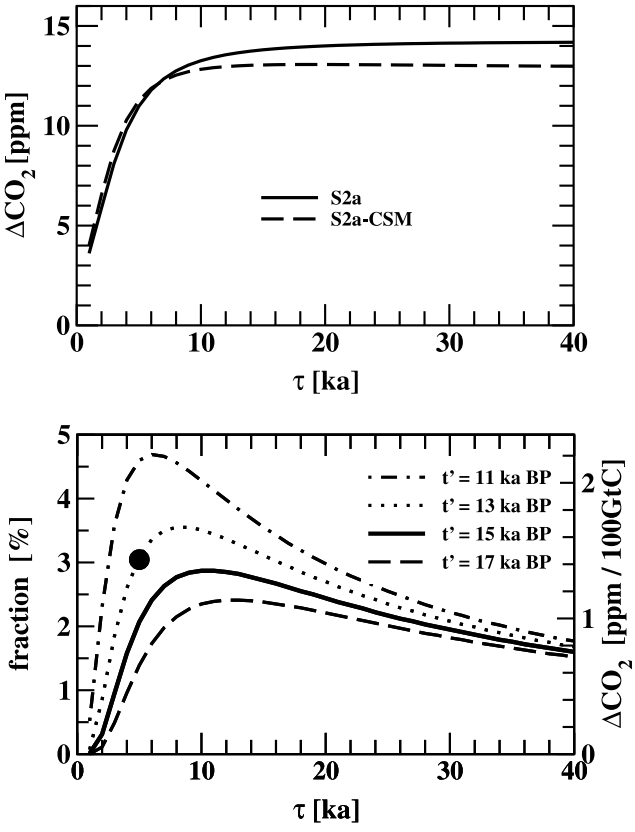

Figure 7. (top) CO_2 increase (8 to 0 ka BP) by $CaCO_3$ compensation. The timescale τ that governs sediment compensation has been varied between 1 and 40 ka in steps of 1 ka for both the UM (simulation S2a, solid line) and the CSM anomalies (simulation S2a-CSM, dashed line). (bottom) Fraction available for sediment compensation in the period 8 to 0 ka BP. The fraction has been calculated from equation (1) as a function of τ and the time of the terrestrial carbon uptake, t'. The solid circle gives the fraction that is compensated between 8 and 0 ka BP for the standard simulation S1 as calculated by dividing the atmospheric increase of 11 ppm by the terrestrial uptake of 781 GtC $\times$ 0.47 ppm/GtC for 21 to 8 ka BP (Table 2). An e-folding timescale of 5 ka is applied in the standard simulation S1.

(Figure 8) than the standard simulation S1. This is incompatible with observations. Sediment compensation, which partly compensates the terrestrial uptake during 10.5 to 8 ka BP in the standard simulation S1, is strongly reduced in S4. After 8 ka BP, the growth rates in atmospheric CO_2 are similar as in the standard simulation and only slightly lower than observed. A terrestrial carbon release during the past 8 ka is mainly responsible for the CO_2 increase in S4.

[42] In simulation S5, we kept the CO_2 concentration in the model's photosynthesis module constant at 267 ppm after 10.5 ka BP. Thereby, fertilization occurs during the deglaciation, but further CO_2 fertilization during the Holocene is prevented. The simulated decrease in CO_2 at the beginning of the Holocene is still larger than in the standard simulation and in the data (Figure 8). However, the terrestrial release in combination with $CaCO_3$ compensation of the uptake during the deglaciation and the early Holocene results in a total CO_2 increase of 20 ppm after 8 ka BP, which is consistent with the ice core data.

[43] Simulations S1 and S4 lead us to several conclusions. First, S4 (with inhibited CO_2 fertilization) is compatible with the *Indermühle et al.* [1999] hypothesis that terrestrial release in combination with sea surface warming caused atmospheric CO_2 to rise during the past 8 ka. However, the modeled change in terrestrial storage during the deglaciation and the early Holocene (Table 2, simulation P2) in S4 was lower than data-based reconstructions, and the CO_2 drawdown in the early Holocene was overestimated by $\sim$4 ppm. Second, the magnitude of the CO_2 fertilization mechanism as implemented in LPJ appears not to be critical in order to simulate the observed CO_2 increase after 8 ka

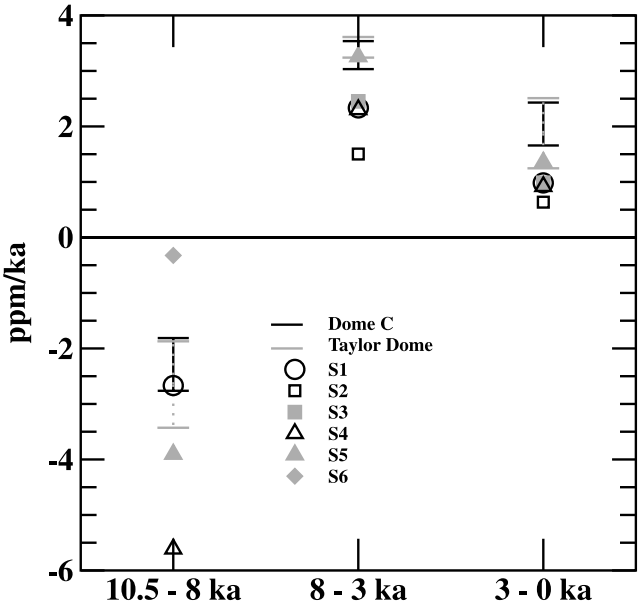

Figure 8. Reconstructed versus simulated atmospheric CO_2 growth rates. The average growth rates have been estimated with linear regression for different Holocene periods for both the Dome C (black solid error bar) [*Flückiger et al.*, 2002] and the Taylor Dome (shaded error bar) [*Indermühle et al.*, 1999]. The bars denote 1 standard deviation determined from the error of the estimated slope, taking into account the analytical uncertainties of the data. Modeled growth rates are given for the standard simulation (S1, solid circle), the simulations S2 with $CaCO_3$ compensation only after 8 ka BP (open square), the simulation S3 (solid square) where only $CaCO_3$ compensation and SST changes are considered after 8 ka BP, while terrestrial storage is kept constant, simulation S4 (open triangle) where CO_2 fertilization is suppressed over the entire 21 ka period, simulation S5 (solid triangle) where CO_2 fertilization is suppressed during the Holocene only, and simulation S6 (solid diamond) where ice sheet extent is kept constant after 10.5 ka BP.

BP, but has implications for the mechanistic explanation of the increase. In the standard simulation S1, $CaCO_3$ compensation is the dominant process explaining about half of the observed increase. In S4, with CO_2 fertilization suppressed, terrestrial carbon release was the dominant process and the role of $CaCO_3$ compensation was less. The simulated changes in terrestrial storage between the LGM and pre-industrial times, 820 GtC in S1, 100 GtC in S4, span more than the range of 300 to 700 GtC derived from $\delta^{13}C$ mass balance calculations. Hence the two simulations might roughly be considered as providing upper and lower limits for the strength of the $CaCO_3$ compensation mechanism.

3.2.5. Ice Sheet Retreat

[44] The decrease in atmospheric CO_2 between 10.5 and 8.5 ka is mainly caused by the establishment of boreal forest following ice sheet retreat. This is demonstrated by simulation S6, where vegetation has been prevented from growing on formerly ice-covered land. Simulated atmospheric CO_2 decreases only by about 1 ppm during the early Holocene in S6, compared to a 6 ppm decrease in the standard simulation and in the ice core data. As noted above, terrestrial uptake on formerly ice-covered land is partly off-set by sediment compensation. In this simulation, SST changes contribute little to the simulated CO_2 changes between 10.5 and 8 ka BP.

3.3. Holocene Atmospheric $\delta^{13}C$

[45] Atmospheric $^{13}CO_2$ has the potential to give additional constraints on carbon cycle processes governing the evolution of atmospheric CO_2 during the Holocene [*Indermühle et al.*, 1999]. Fluxes associated with the $CaCO_3$ sedimentation have a very small impact on atmospheric $\delta^{13}C$, whereas terrestrial carbon release and sea-surface warming both tend to increase atmospheric $\delta^{13}C$. Simulated atmospheric $\delta^{13}C$ increases by 0.2‰ from 10.5 ka BP until about 6 ka BP, in response to terrestrial uptake and sea surface warming (simulation S1; Figure 9). After 6 ka BP, $\delta^{13}C$ remains relatively stable. Small changes were also found by *Brovkin et al.* [2002]. The amplitude of the simulated $\delta^{13}C$ changes is small compared to the data range of about 0.4‰. Sea surface warming causes $\delta^{13}C$ to increase by 0.07‰ after 8 ka BP (simulation S3). Simulation S4 with suppressed CO_2 fertilization yields a decrease of slightly more than 0.1‰ after 5 ka BP, caused by terrestrial release. These results illustrate the fact that the precision of $\delta^{13}C$ data needs to be ±0.1‰ or better for a reliable separation of land and ocean processes.

3.4. Mean Changes in Oceanic $\delta^{13}C$

[46] Release of isotopically light, organic carbon leads to a lower $\delta^{13}C$ signature in the ocean and in the whole ocean-atmosphere-land biosphere-reactive sediment system. The mean $\delta^{13}C$ signature of dissolved inorganic carbon (DIC) in the ocean was lower during the LGM as compared to today, consistent with a lower terrestrial carbon inventory at the LGM. *Duplessy et al.* [1988] estimate from marine sediment data that $\delta^{13}C$ of DIC was on average lower by 0.32‰ over the water column in the Pacific. *Curry et al.* [1988] estimate LGM-Holocene changes in the deep water isotopic composition between 0.28‰ (Indian) and 0.81‰ (Southern Ocean) and a mean deep ocean change of 0.46‰. These numbers have been used to estimate the LGM-Holocene change in terrestrial carbon stocks to be 300 to 700 GtC [*Bird et al.*, 1994, 1996].

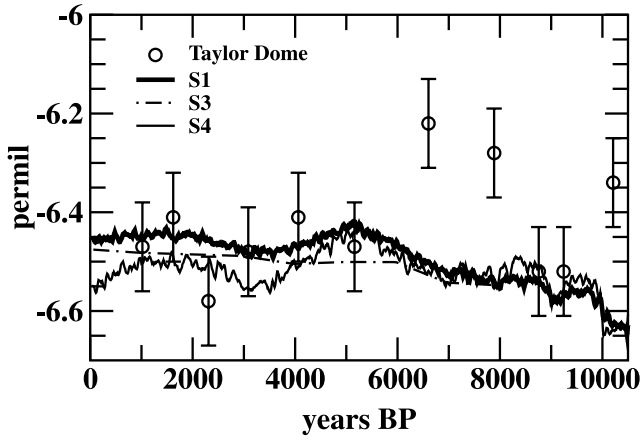

Figure 9. Simulated $\delta^{13}C$ in atmospheric CO_2 versus the Holocene $\delta^{13}C$ ice core record. Ice core data are from Taylor Dome (circle) [*Indermühle et al.*, 1999], and the error bars are estimates of their reproducibility (1 standard deviation). Model results are from the standard simulation (S1, thick solid line), simulation S3 where SST changes and $CaCO_3$ compensation only is considered after 8 ka BP, and simulation S4 where CO_2 fertilization is suppressed. Atmospheric $\delta^{13}C$ is only simulated after 8 ka BP in Simulation S3. Results have been smoothed by 50-year running means.

[47] We estimated the temporal evolution of the average $\delta^{13}C$ signature of DIC from the modeled terrestrial changes in carbon and ^{13}C, taking into account changes in the distribution of C_3 and C_4 plants, changes in the air-biota isotopic fractionation, net export of carbon and carbon isotopes by sedimentary burial, and dilution of the isotopic perturbation by the atmosphere, by the land biosphere, by the reactive ocean sediment layer, and by the marine carbon pools, but neglecting changes in the size of the marine organic carbon pool (see Appendix B). Modeled $\delta^{13}C$ of DIC is 0.50‰ lower at the LGM than today for the standard case where simulated terrestrial storage was 820 GtC lower at the LGM (simulation P1) (Figure 10, bottom).

[48] Changes in the mean terrestrial isotopic signature have a minor impact on the modeled changes in $\delta^{13}C$ of DIC. The reason is that the biospheric C inventory is about 15 times smaller than the total carbon inventory in the ocean-atmosphere-land biosphere-reactive sediment system. The simulated mean $\delta^{13}C$ difference between the terrestrial and atmospheric carbon stocks decreased by 1.1‰ from the LGM to the Holocene (Figure 10, top; simulation P1). An increase in boreal trees that leads to a higher ratio of carbon assimilated by C_3 versus C_4 plants has contributed to this shift. The estimated oceanic $\delta^{13}C$ shift is 0.05‰ smaller than in the standard case, if the land biosphere-atmosphere $\delta^{13}C$ difference is kept at the Holo-

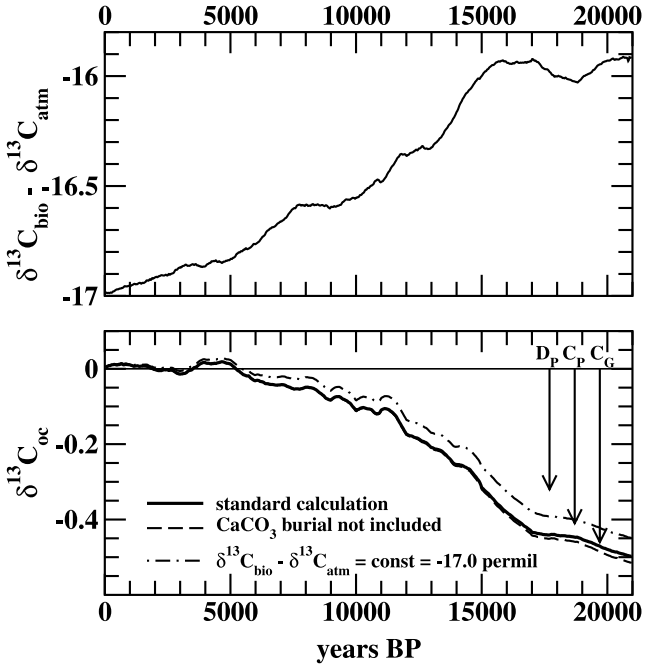

Figure 10. Modeled LGM-Holocene changes (top) in the mean $\delta^{13}C$ difference between the terrestrial and atmospheric carbon stocks and (bottom) in the average isotopic signature of the carbon stored in the ocean-atmosphere-land-reactive sediment system (solid line). Values are for simulation P1 and in permil units. Changes in the atmosphere-land biosphere $\delta^{13}C$ difference and the export of carbon by sediment burial have a small influence on the modeled oceanic $\delta^{13}C$ perturbation as illustrated by calculations where the atmosphere-land biosphere $\delta^{13}C$ difference was kept constant (dash-dotted line) or calcite burial neglected (dashed line). Thin arrows indicate data-based estimates of the average LGM-Holocene change for the whole Pacific (D_P, [*Duplessy et al.*, 1988]), and for deep waters only in the Pacific (C_P) and globally (C_G) [*Curry et al.*, 1988].

cene value of −17‰. Even smaller deviations relative to the standard are found when carbon export to ocean sediments is neglected.

[49] A major caveat in the above calculations is the unknown fate of the marine organic carbon pool. Marine organic carbon has a similar isotopic signature to the organic carbon on land. Hence the observed isotopic change in marine sediments is only indicative of the total net change in organic carbon, but allows no distinction between changes in the oceanic versus the terrestrial organic pools. Here we have assumed that the organic carbon pool of 700 GtC remained constant over time, similar to calculations of terrestrial carbon stock changes [*Bird et al.*, 1994, 1996]. Marine sediment $\delta^{13}C$ data and our modeled estimate of the mean oceanic $\delta^{13}C$ change would come into agreement if the organic carbon pool in the ocean was larger by 100 to 500 GtC at the LGM than today.

3.5. Changes in Plant Type Distribution

[50] Vegetation reconstructions based on pollen and plant macrofossil data show that global biome distributions at the LGM were markedly different from present [*Wright et al.*, 1993; *Prentice et al.*, 2000]. The differences can be broadly explained by the presence of ice sheets, a global reduction in land-surface temperature, and a reduced water cycle in concert with lower C_3 plant productivity and plant water-use efficiency directly due to the low atmospheric CO_2 concentration [*Harrison and Prentice*, 2003]. Vegetation reconstructions also show differences between mid-Holocene and present biomes [*Wright et al.*, 1993; *Prentice et al.*, 2000], although these are less extensive at a global scale. In order to assign the simulated abundances of the PFTs to biome types, we use the simple algorithm summarized in Figure 11. The simulated potential natural vegetation for pre-industrial time (Figure 12) shows the main features indicated in global maps [e.g., *Haxeltine and Prentice*, 1996; *de Fries et al.*, 1999]. The simulated mid-Holocene biome distribution also shows qualitative features of late Holocene vegetation change (Figure 12) as indicated by pollen

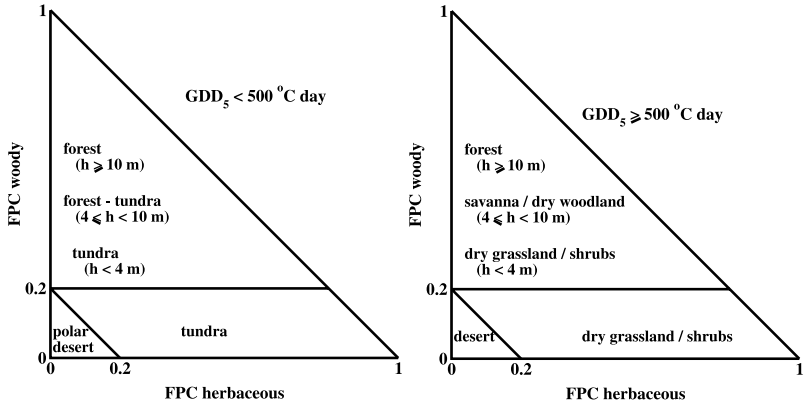

Figure 11. Scheme used to assign biome types from the simulated fractional plant cover (FPC) of woody and herbaceous species and simulated stand height (h).

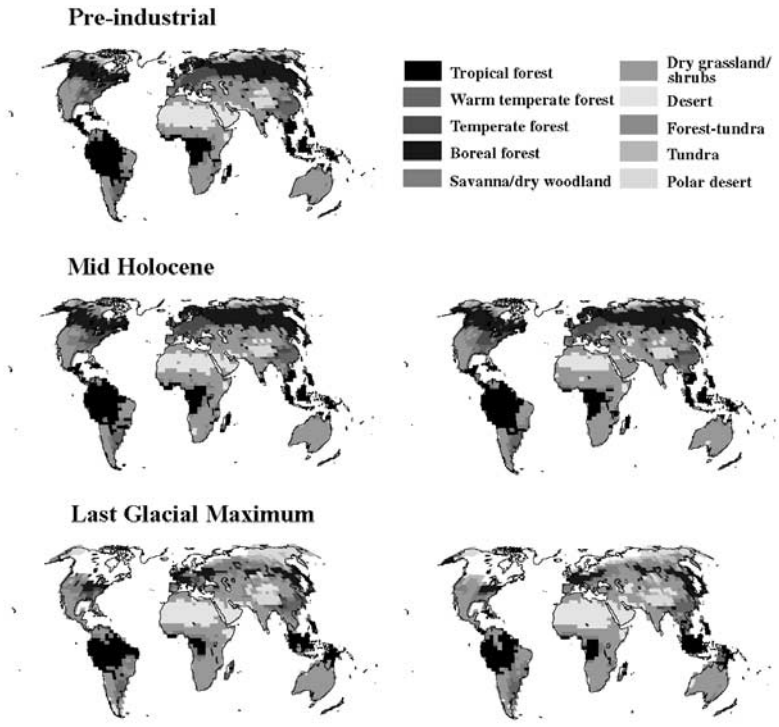

Figure 12. Simulated biome distribution for the LGM (21 ka BP), the Mid-Holocene (6 ka BP), and the pre-industrial time (0 ka) for the UM climate anomalies (left, simulation P1) and the CSM climate anomalies (right, simulation P1-CSM). The distribution at pre-industrial time is nearly identical for simulations with the UM and the CSM anomalies (not shown). See color version of this figure at back of this issue.

analysis data at sampling points, whose density, however, varies considerably among regions [*Prentice et al.*, 2000]. The Central African tropical forest is reduced; this is supported by the limited observational evidence from this region, and has been attributed to a moisture shift of the intertropical convergence zone [*Harrison et al.*, 1998]. A slight simulated increase in precipitation to the north of the Sahel produces a northward encroachment of shrubs and grass into areas which are desert today. This is qualitatively consistent with extensive evidence [*Jolly et al.*, 1998], and can be explained by an increase in monsoon penetration due to the greater than present land-sea contrast in the Northern Hemisphere [*Kutzbach and Street-Perrott*, 1985]. However, the simulated vegetation shift rarely exceeds one latitudinal band (2.5°); the CSM produces a slightly more pronounced northward shift. Neither model reproduces the full magnitude of reduction of the Sahara desert shown by data [*Jolly et al.*, 1998]. This underestimation is to be expected because the UM simulation lacks the positive feedback caused by circulation changes in the Atlantic [*Kutzbach and Liu*, 1997; *Braconnot et al.*, 1999] while the CSM simulation lacks the positive feedback caused by vegetation-atmosphere interactions [e.g., *Broström et al.*, 1998; *Braconnot et al.*, 1999; *de Noblet-Ducoudré et al.*, 2000].

[51] The observed slight northward shift in the arctic treeline [*Prentice et al.*, 2000; *Bigelow et al.*, 2003; *Kaplan et al.*, 2002] is too small to be represented well with the coarse model resolution, but it is indicated by a few grid cells in the northern circumpolar region. In the midlatitudes, few changes in vegetation distribution are simulated. The extent of temperate forest in North America, Europe, and China nearly remain unchanged, and the observed northward extension of temperate treelines in Europe and China [*Prentice et al.*, 2000] is not resolved.

[52] The simulated biome distribution for the LGM differs radically from the present-day or mid-Holocene distribution and reproduces the broad features observed in paleodata. Strong reduction in temperatures in northern latitudes produced a southward displacement and major reduction in area of the boreal forest, while reduced precipitation over midlatitude Eurasia caused a fragmentation of the temperate forests. These features are consistent with observations, as summarized, for example, by *Prentice et al.* [2000]. However, despite the reduced precipitation, the simulations show forest over much of western Europe whereas the data show even drier conditions with steppe predominant. The reconstructions also show a reduced extent of tropical forests and increased extent of grasslands and shrublands. The UM especially appears to overestimate low-latitude tree cover.

[53] In conclusion, the main changes in simulated and reconstructed biome distributions agree moderately well with data for the LGM and the mid-Holocene. The largest

differences arise in the tropics, where the simulated extent of tropical forests is overestimated at the time of the LGM, and the modeled reduction of the Sahara desert is underestimated in mid-Holocene time.

4. Potential Impact of Land Use Emissions

[54] The grand hypothesis by *Ruddiman* [2003] that human activities prevented the climate system to enter a glacial during the Holocene has been discussed in two editorials [*Crowley*, 2003; *Crutzen and Steffen*, 2003]. A part of the hypothesis is that land use prevented atmospheric CO_2 to drop and that anthropogenic land use emissions are responsible for a 40 ppm atmospheric anomaly. In the following we scrutinize this part of the overall hypothesis.

[55] First, we estimate a lower limit for the anthropogenic emissions needed to raise atmospheric CO_2 by 40 ppm over the Holocene. The ocean is roughly in equilibrium with the atmosphere on a millennial timescale, and about 85% of the carbon emission into the atmosphere must have been removed by the ocean, leaving only ~15% airborne (Figure 1). This yields a cumulative carbon emission by land use of 566 ppm (40 ppm $\times$ 2.123 GtC ppm^{-1} $\times$ 100/15). The effective emissions to explain a 40 ppm rise must be higher as ocean sediment interaction would have further reduced the atmospheric perturbation. We note that the equilibrium airborne fraction is well constrained, as ocean carbonate chemistry and ocean volume, the two primary governing factors, are well known. Second, a lower limit for the atmospheric $\delta^{13}C$ perturbation is estimated by applying equation B2 of Appendix B. This yields a decrease in atmospheric $\delta^{13}C$ of 0.3‰. Third, a transient simulation with HILDA model (coupled to the IRF sediment model and a box-type biosphere) is carried out to take into account system dynamics. Prescribing a linear increase from 240 to 280 ppm over the past 8 ka yields a cumulative carbon emission of 710 GtC and an atmospheric δ^{13} decrease of 0.6‰.

[56] Both the isotopic perturbation and the carbon emissions by land use implied by the Ruddiman hypothesis are in conflict with other data. The 0.6‰ isotopic perturbation is not compatible with the ice core data that suggest an atmospheric $\delta^{13}C$ decrease of about 0.25‰ during the last 8 ka (Figure 9). Historical cumulative carbon losses due to changes in land use have been estimated to be 180 to 200 GtC by comparing carbon storage for natural vegetation distribution and present-day land cover [*Matthews*, 1983; *de Fries et al.*, 1999]. This is 3 to 4 times less than required for a millennial-scale 40 ppm increase.

[57] Early human-induced land use change might have contributed by a few ppm to the observed pre-industrial CO_2 rise. World population increased by more than an order of magnitude from about 300 million to 5 billion during the last millennium. The vast majority of the population increase occurred during the past 150 years, driving a land use flux of about 120 GtC [*Houghton*, 1999]. Subtracting this estimate from the estimated 180 to 200 GtC total cumulative land use loss yields a pre-1850 emission of 60 to 80 GtC. Such an emission causes atmospheric CO_2, after re-equilibration with the ocean, to rise by 4 to 6 ppm (60 to 80 GtC $\times$ 0.47 ppm/GtC $\times$ 0.15). In conclusion, it is unlikely that the small population that lived during the Holocene could have forced a CO_2 rise of more than a few ppm.

5. Discussion and Conclusions

[58] Possible mechanisms responsible for the evolution of Holocene atmospheric CO_2 are explored by forcing the Bern CC carbon cycle model, which includes the Lund-Potsdam-Jena Dynamic Global Vegetation Model and an ocean-sediment component, with results from time-slice simulations from comprehensive climate models over the past 21 ka. The focus is on terrestrial carbon storage, calcite compensation, and changes in SST, whereas the buildup of coral reefs, peat formation, and anthropogenic land use activities have not been included in the model. The simulated atmospheric CO_2 concentrations match the ice core data within a few ppm and the model results are broadly consistent with proxy data of atmospheric $^{13}CO_2$, mean ocean $\delta^{13}C$, and pollen data, within their uncertainties.

[59] $CaCO_3$ compensation and SST increase are the main factors driving the simulated CO_2 increase during the past 8 ka. Carbon uptake on formerly ice-covered land, partly compensated by a loss of terrestrial carbon due to sea level rise and $CaCO_3$ compensation, is responsible for the simulated early Holocene decrease of CO_2. This conclusion differs from that of *Broecker et al.* [2001], who assigned the entire late Holocene CO_2 increase to sediment compensation, or *Indermühle et al.* [1999], who postulated a terrestrial carbon release as the main cause.

[60] A conceivable alternative explanation emerges when considering the results from simulations in which the CO_2 fertilization mechanism is suppressed. In this case, a terrestrial carbon release in response to temperature and precipitation changes in combination with sea-surface warming and sediment compensation explains the 20 ppm CO_2 increase during the past 8 ka. This result is qualitatively consistent with the proposal by *Indermühle et al.* [1999]. However, the early Holocene CO_2 decrease is overestimated in the simulation by 4 ppm, and total terrestrial uptake during the past 21 ka is only about 100 GtC for the past 21 ka, well below any recent estimate.

[61] Sensitivity analyses and a comparison with data-based reconstructions of the terrestrial uptake suggest that only about half of the observed CO_2 increase of 20 ppm (8 to 0 ka BP) can be explained by $CaCO_3$ compensation in response to earlier terrestrial carbon uptake. The impact of sediment compensation on atmospheric CO_2 during the past 8 ka is principally determined by the total amount of terrestrial carbon uptake during the glacial-interglacial transition and the early Holocene. We find that its contribution to the atmospheric CO_2 increase between 8 and 0 ka BP corresponds to 3 $\pm$ 1% of this terrestrial uptake. The data-based range of 300 to 700 GtC implies a late Holocene CO_2 rise between 4 and 10 ppm (3% $\times$ 0.47 ppm/GtC $\times$ 300 to 700 GtC) due to this mechanism.

[62] A relatively strong contribution to the Holocene CO_2 rise by SST change is found here in contrast to *Brovkin et al.* [2002], who suggest a negligible contribution by this

mechanism. *Brovkin et al.* [2002] applied a model of intermediate complexity, neglecting forcing by ice sheet retreat. Here a box-type ocean model is forced by spatially averaged SST changes obtained from the output of the HadSM3 atmosphere model coupled to a slab ocean model, a sea-ice model, and prescribed orbital, greenhouse gas, and ice sheet forcing. Our results might be biased toward high values as communication between the surface and the deep ocean is not represented by the slab model, and results are influenced by a change in the land-sea mask between 7 and 6 ka in the UM time slice simulations. The contribution of SST changes to the Holocene CO_2 rise requires further investigations.

[63] The hypothesis by *Ruddiman* [2003] that land use prevented atmospheric CO_2 from dropping and that anthropogenic land use emissions are responsible for a 40 ppm increase is dismissed based on the ice core $\delta^{13}C$ record and other well-founded land use emission estimates [*Matthews*, 1983; *de Fries et al.*, 1999]. We estimate that early human-induced land use emissions might have contributed 4 to 6 ppm to the observed CO_2 rise.

[64] Other processes not represented in our simulations might have contributed to the Holocene CO_2 evolution. (1) *Ridgwell et al.* [2003] show that coral reef buildup is likely to play an important role for the late Holocene CO_2 evolution. (2) Beside $CaCO_3$ compensation of terrestrial uptake and coral reef buildup, other sediment-ocean interactions have the potential to increase atmospheric CO_2 during the Holocene. These include changes in the rain-ratio of calcite and organic carbon and changes in the silica cycle in response to the glacial-interglacial reorganization [*Archer and Maier-Reimer*, 1994; *Matsumoto et al.*, 2002]. (3) The greening of the Sahara desert as reconstructed for 6 ka BP is not simulated in our model setup, similar to other models that do not include climate-vegetation feedbacks. However, *Indermühle et al.* [1999] estimated that the desertification of the Sahara caused a terrestrial release of about 30 GtC during the past 6 ka (until pre-industrial time). This implies that only 2 ppm of the rise can be explained by the Late Holocene expansion of the Sahara. (4) Long-term changes in solar irradiance, which were not considered in the UM and CSM simulations, might conceivably have contributed to a warmer climate and to a terrestrial release of a few ppm. *Gerber et al.* [2003] suggested that solar irradiance changes caused atmospheric CO_2 variations of about 6 ppm during the last millennium. However, the residual ^{14}C tree ring record [*Stuiver et al.*, 1998] suggests little long-term changes in solar irradiance. (5) The 8.2 ka cold event in the North Atlantic region, not represented in the UM and CSM simulations, might have caused additional terrestrial uptake of up to a few tens of GtC around 8.2 ka BP and a subsequent release thereafter. (6) On the other hand, peat buildup in high northern latitudes may have sequestered additional carbon on land. A recent estimate [*Gajewski et al.*, 2001, 2002] suggests that about 400 GtC have been stored in northern peat land during the past 8 ka and 200 to 320 GtC during the past 3 ka. Such high estimates are, however, in conflict with the ice core records for atmospheric CO_2 and $\delta^{13}C$.

[65] In summary, the early Holocene CO_2 decrease has been quantitatively explained by terrestrial uptake and calcite compensation. CO_2 fertilization and forest growth on formerly ice covered areas are mainly responsible for the simulated uptake of 820–850 GtC over the past 21 ka, whereas changes in climate alone would lead to a terrestrial carbon loss. A range of mechanisms, including calcite compensation, terrestrial carbon uptake and release, SST changes, and coral reef buildup, contributed to the 20 ppm late Holocene CO_2 rise. We constrained the contribution of calcite compensation (in response to terrestrial uptake during the transition and the early Holocene) to 4 to 10 ppm. Terrestrial carbon inventory changes related to climate and CO_2 forcing, the greening of the Sahara, peat buildup, and land use have probably influenced CO_2 by a few ppm only. SST variations contributed between 0 and 6 ppm. The land use scenario by [*Ruddiman*, 2003] is highly unlikely and not compatible with the ice core $\delta^{13}C$ record. The potentially large contribution of coral reef buildup needs to be further explored with 3-D ocean-sediment models.

[66] A high-precision ice core $\delta^{13}C$ record with a high temporal resolution would have the potential to shed further light on the Holocene CO_2 problem. Our simulations suggest that the precision of the record must be better than 0.1‰.

Appendix A: Representation of $CaCO_3$ Compensation

[67] The IRF substitute for the HILDA ocean model is described elsewhere [*Joos et al.*, 1996, 2001]. Here these equations are complemented by an IRF representation of the impact of $CaCO_3$ sediment compensation on atmospheric CO_2 [*Archer et al.*, 1997].

[68] $CaCO_3$ dissolution and sedimentation affects both the balance of dissolved inorganic carbon (DIC, ΣCO_2) and of alkalinity in the ocean. For simplicity, the impact of alkalinity changes on the partial pressure of CO_2 and atmospheric CO_2 is formally factored into changes in the concentration of DIC, here termed $\delta\Sigma CO_2^*$. The asterisk superscript refers to the inclusion of the impact of alkalinity changes, and δ denotes the change since the start of the simulation. This simplification does not affect simulated atmospheric CO_2.

[69] The flux of ΣCO_2^* from the sediment (*sed*) to the ocean (*oc*) is given by the convolution integral

$$F_{sed,oc}(t) = \int_{t_0}^{t} dt' \frac{a}{\tau} F_{a-oc,out}(t')\, e^{-\frac{t-t'}{\tau}}, \qquad \text{(A1)}$$

where $F_{a-oc,out}$ is the net flux of carbon leaving the ocean-atmosphere system. For example, $F_{a-oc,out}$ is the net flux into the terrestrial biosphere minus fossil carbon emissions. Here t_0 denotes the time at the start of the simulation, and a denotes the fraction of the ocean-atmosphere perturbation that is eventually removed by $CaCO_3$ compensation with the governing timescale τ. The values of a and τ are set to 0.7 and 5000 years in the standard model setup [*Archer et al.*, 1997]. The convolution integral is reformulated for computational efficiency, and the flux from the sediment at

Table A1. Timscales and Coefficients for the Sediment Compensation IRF

		a_i		
i	τ_i, years	Mean	Fast	Slow
1	5500	0.54	0.6	0.4
2	8200	0.14	0.1	0.28
3	200,000	0.32	0.3	0.32

time t is calculated from the flux from the sediment at the previous time step and the net flux leaving the system,

$$F_{sed,oc}(t) = F_{sed,oc}(t-\Delta t)e^{-\frac{\Delta t}{\tau}} + \frac{\Delta t\, a}{\tau} F_{a-oc,out}(t-\Delta t)e^{-\frac{\Delta t}{\tau}}, \quad \text{(A2)}$$

where Δt is the length of the model time step.

[70] The multicentury timescale of ocean overturning is small compared to the timescale of sediment compensation, and the $\Sigma CO_2^*(t)$ concentration is uniformly lowered throughout the ocean,

$$\delta\Sigma CO_2^*(t) = \delta\Sigma CO_2^*(t-\Delta t) + \frac{10^6}{V_{oc}\,\rho} F_{sed,oc}(t)\,\Delta t. \quad \text{(A3)}$$

Here, V_{oc} is the ocean volume ($1.38\ 10^{18}$ m^3) and ρ is the density of ocean water. $F_{sed,oc}$ and $F_{a-oc,out}$ are in units of mol yr^{-1} (1 GtC = $8.33\ 10^{13}$ mol), and $\delta\Sigma CO_2^*$ is in units of μmol kg^{-1}. $F_{sed,oc}$ and $\delta\Sigma CO_2^*$ are initialized to zero at the start of the transient simulation. This change in DIC due to sediment compensation, $\delta\Sigma CO_2^*(t)$, is added to the change in DIC due to air-sea gas exchange in the HILDA IRF model [*Joos et al.*, 1996, equation (3)] before evaluating sea surface partial pressure.

[71] In sensitivity experiments, the IRF is refined, according to the timescales given by *Archer et al.* [1997]. Then equation (A1) changes to

$$F_{sed,oc}(t) = \int_{t_0}^{t} \sum_{i=1}^{3} \frac{a_i}{\tau_i} F_{a-oc,out}(t') e^{-\frac{t-t'}{\tau_i}} dt'. \quad \text{(A4)}$$

[72] Uncertainties associated with the a_i are considered by determining a "fast" compensation, where a_1 is set to the highest feasible value and a_3 to the lowest, and a "slow" compensation, with a_1 low and a_3 high. Here a_2 is set that $\Sigma a_i = 1$. The coefficients applied are given in Table A1.

Appendix B: Mean Ocean $\delta^{13}C$ Signature

[73] Release of isotopically light organic carbon perturbs the isotopic signal in the relatively fast (<1000 years) exchanging carbon reservoirs, land biosphere, atmosphere, ocean, and reactive sediments. This perturbation is calculated from the modeled changes in the terrestrial carbon stock and the modeled changes in the mean land biosphere-atmosphere $\delta^{13}C$ difference, $\delta^{13}C_{b-a}$.

[74] The mass balance for ^{13}C is [*Heimann and Maier-Reimer*, 1996]

$$\frac{d}{dt}\left[N_a \cdot \delta^{13}C_a + N_b \cdot \delta^{13}C_b + N_{o,DIC} \cdot \delta^{13}C_{o,DIC} + N_{o,OC} \cdot \delta^{13}C_{o,OC} + N_{rs} \cdot \delta^{13}C_{rs}\right] - F_w \cdot \delta^{13}C_w + F_s \cdot \delta^{13}C_s = 0, \quad \text{(B1)}$$

where N denotes a carbon inventory, $\delta^{13}C$ is the $^{13}C/^{12}C$ isotopic ratio expressed in permil units, the indices a, b, o, and rs refer to the atmosphere, biosphere, ocean, and reactive sediments, DIC is dissolved inorganic carbon, OC is organic carbon, F_w is the carbon input by weathering, F_s the carbon loss by burial, and $\delta^{13}C_w$ and $\delta^{13}C_s$ the isotopic signatures of these fluxes.

[75] Equation (B1) is solved for the mean perturbation in the system, $\Delta\delta^{13}C_m$, by assuming that (1) the pool of organic carbon in the ocean remains constant, (2) its isotopic difference relative to DIC remains constant, (3) the isotopic perturbation in response to the terrestrial change is equal in all reservoirs, (4) the carbon input by weathering is balanced by the loss to the sediment and that the weathering flux is isotopically unperturbed, whereas the burial flux carries the mean isotopic perturbation, and (5) $\delta^{13}C$ changes other than those from the terrestrial perturbation, for example, due to SST changes or changes in the marine biological cycle, can be neglected [*Smith et al.*, 1999]. The estimated overall LGM to Holocene $\Delta\delta^{13}C_m$ change is not sensitive to assumptions (2) to (5) within reasonable, data-based limits, whereas a change in the isotopically depleted organic carbon inventory in the ocean would influence the results similarly as an equal change in the terrestrial carbon inventory. This yields

$$\begin{aligned}\frac{d}{dt}\Delta\delta^{13}C_m = {} & \frac{-1}{N_a + N_b + N_{o,DIC} + N_{o,OC} + N_{rs}} \\ & \cdot \Big[\left(\delta^{13}C_{a,0} + \Delta\delta^{13}C_m\right) \cdot \frac{d}{dt}N_a + \left(\delta^{13}C_{a,0} + \delta^{13}C_{b-a} \right. \\ & \left. + \Delta\delta^{13}C_m\right) \cdot \frac{d}{dt}N_b + N_b \cdot \frac{d}{dt}\delta^{13}C_{b-a} \\ & + \left(\delta^{13}C_{o,DIC,0} + \Delta\delta^{13}C_m\right) \cdot \frac{d}{dt}N_{o,DIC} \\ & + \left(\delta^{13}C_{rs,0} + \Delta\delta^{13}C_m\right) \cdot \frac{d}{dt}N_{rs} + F_s \cdot \Delta\delta^{13}C_m\Big].\end{aligned} \quad \text{(B2)}$$

[76] Equation (B2) is evaluated backward in time for a pre-industrial atmospheric signature, $\delta^{13}C_{a,0}$, of -6.4‰, the modeled land-atmosphere isotopic difference, $\delta^{13}C_{b-a}$ (Figure 10, top), the pre-industrial signatures of DIC and of reactive sediments of 0‰, a total carbon inventory of 43'020 GtC ($N_{a,0}$ = 600 GtC; $N_{b,0}$ = 2'920 GtC; $N_{oc,DIC,0}$ = 38'000 GtC; $N_{oc,OC,0}$ = 700 GtC; $N_{rs,0}$ = 800 GtC), the prescribed change in the atmospheric carbon inventory from the ice core data, the modeled change in the terrestrial carbon inventory (Figure 4, top), a burial flux of 0.2 GtC yr^{-1}, and by setting the combined change in the DIC and reactive sediment carbon inventories equal to the change in the atmospheric plus terrestrial inventory.

[77] **Acknowledgments.** This work is funded by the Swiss National Science Foundation. Jed Kaplan is thanked for providing input data. David Archer and Niki Gruber are thanked for their helpful reviews, and Michel Crucifix and Viktor Brovkin are thanked for comments on the manuscript. Discussions with Andy Ridgwell, Jed Kaplan, Corinne Le Quéré, Wolfgang Knorr, and other members of the LPJ model development team were enjoyed.

References

Adams, J. M., and H. Faure (1998), A new estimate of changing carbon storage on land since the Last Glacial Maximum, based on global land ecosystem reconstruction, *Global Planet. Change*, *16–17*, 3–24.

Adams, J. M., H. Faure, L. Faure-Denard, J. M. McGlade, and F. I. Woodward (1990), Increase in terrestrial carbon storage from the Last Glacial Maximum to the present, *Nature*, *348*, 711–714.

Archer, D., and E. Maier-Reimer (1994), Effect of deep-sea sedimentary calcite preservation on atmospheric CO_2 concentration, *Nature*, *367*, 260–263.

Archer, D., H. Keshgi, and E. Maier-Reimer (1997), Multiple timescales for neutralization of fossil fuel CO_2, *Geophys. Res. Lett.*, *24*, 405–408.

Archer, D., A. Winguth, D. Lea, and N. Mahowald (2000), What caused the glacial/interglacial atmospheric pCO_2 cycles?, *Rev. Geophys.*, *38*, 159–189.

Beerling, D. J. (1999), New estimates of carbon transfer to terrestrial ecosystems between the Last Glacial Maximum and the Holocene, *Terra Nova*, *11*, 162–167.

Beerling, D. J. (2000), The role of the terrestrial biosphere in Holocene carbon cycle dynamics, *Global Ecol. Biogeogr.*, *9*, 421–429.

Bennett, K. D., and K. J. Willis (2000), Effect of global atmospheric carbon dioxide on glacial-interglacial vegetation change, *Global Ecol. Biogeogr.*, *9*, 355–361.

Bigelow, N. H., et al. (2003), Climate change and Arctic ecosystems: 1. Vegetation changes north of 55°N between the Last Glacial Maximum, mid-Holocene and present, *J. Geophys. Res.*, *108*(D19), 8170, doi:10.1029/2002JD002558.

Bird, M. I., J. Lloyd, and G. D. Farquhar (1994), Terrestrial carbon storage at the LGM, *Nature*, *371*, 566.

Bird, M. I., J. Lloyd, and G. D. Farquhar (1996), Terrestrial carbon-storage from the Last Glacial Maximum to the present, *Chemosphere*, *33*, 1675–1685.

Boville, B. A., and P. R. Gent (1998), The NCAR climate system model, version one, *J. Clim.*, *11*, 1115–1130.

Braconnot, P., S. Joussaume, O. Marti, and N. de Noblet (1999), Synergistic feedbacks from ocean and vegetation on the African monsoon response to mid-Holocene insolation, *Geophys. Res. Lett.*, *26*, 2481–2484.

Broecker, W. S., and E. Clark (2003), Holocene atmospheric CO_2 increase as viewed from the seafloor, *Global Biogeochem. Cycles.*, *17*, 1052, doi:10.1029/2002GB001985.

Broecker, W. S., and T.-H. Peng (1987), The role of $CaCO_3$ compensation in the glacial to interglacial atmospheric CO_2 change, *Global Biogeochem. Cycles*, *1*, 15–39.

Broecker, W. S., J. Lynch-Stieglitz, E. Clark, I. Hajdas, and G. Bonani (2001), What caused the atmosphere's CO_2 content to rise during the last 8000 years?, *Geochem. Geophys. Geosyst.*, *2*, Paper number 2001GC00177.

Broström, A., M. Coe, S. P. Harrison, R. Gallimore, J. E. Kutzbach, J. Foley, I. C. Prentice, and P. Behling (1998), Land-surface processes and paleomonsoons in northern Africa, *Geophys. Res. Lett.*, *25*, 3615–3618.

Brovkin, V., J. Bendtsen, M. Claussen, A. Ganopolski, C. Kubatzki, V. Petoukhov, and A. Andreev (2002), Carbon cycle, vegetation, and climate dynamics in the Holocene: Experiments with the CLIMBER-2 model, *Global Biogeochem. Cycles.*, *16*, 1139, doi:10.1029/2001GB001662.

Cowling, S. A., and C. B. Field (2003), Environmental control of leaf area production: implications for vegetation and land-surface modeling, *Global Biogeochem. Cycles.*, *17*, 1007, doi:10.1029/2002GB001915.

Cramer, W., et al. (2001), Global response of terrestrial ecosystem structure and function to CO_2 and climate change: Results from six global dynamic vegetation models, *Global Change Biol.*, *7*, 357–373.

Crowley, T. J. (1991), Ice age carbon, *Nature*, *352*, 575–576.

Crowley, T. J. (1995), Ice-age terrestrial carbon changes revisited, *Global Biogeochem. Cycles*, *9*, 377–389.

Crowley, T. J. (2003), When did global warming start? An editorial comment, *Clim. Change*, *61*, 259–260.

Crutzen, P. J., and W. Steffen (2003), How long have we been in the anthropocene era? An editorial comment, *Clim. Change*, *61*, 251–257.

Curry, W. B., J. C. Duplessy, L. D. Labeyrie, and N. J. Shackleton (1988), Changes in the distribution of $\delta^{13}C$ of deep water ΣCO_2 between the last glaciation and the Holocene, *Paleoceanography*, *3*, 317–341.

Dargaville, R. J., et al. (2002), Evaluation of terrestrial carbon cycle models with atmospheric CO_2 measurements: Results from transient simulations considering increasing CO_2, climate, and land-use effects, *Global Biogeochem. Cycles*, *16*, 1092, doi:10.1029/2001GB001426.

de Fries, R. S., C. B. Field, I. Fung, G. J. Collatz, and L. Bounoua (1999), Combining satellite data and biogeochemical models to estimate global effects of human-induced land cover change on carbon emissions and primary productivity, *Global Biogeochem. Cycles*, *13*, 803–815.

DeLucia, E. H., et al. (1999), Net primary production of a forest ecosystem with experimental CO_2 enrichment, *Science*, *284*, 1177–1179.

de Noblet-Ducoudré, N., M. Claussen, and C. Prentice (2000), Mid-Holocene greening of the Sahara: First results of the GAIM 6000 year BP experiment with two asynchronously coupled atmosphere/biome models, *Clim. Dyn.*, *6*, 643–659.

Duplessy, J. C., N. J. Shackleton, R. G. Fairbanks, L. Labeyrie, D. Oppo, and N. Kallel (1988), Deepwater source variations during the last climate cycle and their impact on the global deepwater circulation, *Paleoceanography*, *3*, 343–360.

Esser, G., and M. Lautenschlager (1994), Estimating the change of carbon in the terrestrial biosphere from 18,000 BP to present using a carbon cycle model, *Environ. Pollut.*, *83*, 45–53.

Flückiger, J., E. Monnin, B. Stauffer, J. Schwander, T. F. Stocker, J. Chappellaz, D. Raynaud, and J. M. Barnola (2002), High-resolution Holocene N_2O ice core record and its relationship with CH_4 and CO_2, *Global Biogeochem. Cycles.*, *16*, 1010, doi:10.1029/2001GB001417.

Foley, J. A. (1994), The sensitivity of the terrestrial biosphere to climatic change: A simulation of the middle Holocene, *Global Biogeochem. Cycles*, *8*, 505–525.

François, L. M., C. Delire, P. Warnant, and G. Munhoven (1998), Modelling the glacial-interglacial changes in the continental biosphere, *Global Planet. Change*, *16–17*, 37–52.

François, L. M., Y. Goddéris, P. Warnant, G. Ramstein, N. de Noblet, and S. Lorenz (1999), Carbon stocks and isotopic budgets of the terrestrial biosphere at mid-Holocene and Last Glacial Maximum times, *Chem. Geol.*, *159*, 163–189.

Friedlingstein, P., C. Delire, J. F. Müller, and J. C. Gérard (1992), The climate-induced variation of the continental biosphere: A model simulation of the Last Glacial Maximum, *Geophys. Res. Lett.*, *19*, 897–900.

Friedlingstein, P., K. C. Prentice, I. Y. Fung, and J. G. John (1995), Carbon-biosphere-climate interactions in the Last Glacial Maximum climate, *J. Geophys. Res.*, *100*, 7203–7221.

Gajewski, K., A. Viau, M. Sawada, D. Atkinson, and S. Wilson (2001), Sphagnum peatland distribution in North America and Eurasia during the past 21,000 years, *Global Biogeochem. Cycles*, *15*, 297–310.

Gajewski, K., A. Viau, M. Sawada, D. Atkinson, and S. Wilson (2002), Area and carbon content of Sphagnum since Last Glacial Maximum, in *Trends: A Compendium of Data on Global Change*, Carbon Dioxide Inf. Anal. Cent., Oak Ridge, Tenn.

Gerber, S., F. Joos, P. Brügger, T. F. Stocker, M. E. Mann, S. Sitch, and M. Scholze (2003), Constraining temperature variations over the last millennium by comparing simulated and observed atmospheric CO_2, *Clim. Dyn.*, *20*, doi:10.1007/s00382-002-0270-8, 281–299.

Goyet, C., and A. Poisson (1989), New determination of carbonic acid dissociation constants in seawater as a function of temperature and salinity, *Deep Sea Res.*, *36*(11), 1654–2635.

Harrison, S. P., and C. I. Prentice (2003), Climate and CO_2 controls on global vegetation distribution at the Last Glacial Maximum: Analysis based on palaeovegetation data, biome modeling and palaeoclimate simulation, *Global Change Biol.*, *9*, 983–1004.

Harrison, S. P., D. Jolly, F. Laarif, A. Abe-Ouchi, B. Dong, K. Herterich, C. Hewitt, J. E. Kutzbach, J. Mitchell, N. de Noblet, and P. Valdes (1998), Intercomparison of simulated global vegetation distribution in response to 6 kyr B. P. orbital forcing, *J. Clim.*, *11*, 2721–2742.

Haxeltine, A., and I. C. Prentice (1996), BIOME 3: An equilibrium terrestrial biosphere model based on ecophysiological constraints, resource availability and competition among plant functional types, *Global Biogeochem. Cycles*, *10*, 693–703.

Heimann, M., and E. Maier-Reimer (1996), On the relations between the oceanic uptake of CO_2 and its carbon isotopes, *Global Biogeochem. Cycles*, *10*, 89–110.

Hewitt, C. D., C. A. Senior, and J. F. B. Mitchell (2001), The impact of dynamic sea-ice on the climatology and climate sensitivity of a GCM: A study of past, present, and future climates, *Clim. Dyn.*, *17*, 655–668.

Houghton, R. A. (1999), The annual net flux of carbon to the atmosphere from changes in land use 1850–1990, *Tellus, Ser. B*, *51*, 298–313.

Indermühle, A., et al. (1999), Holocene carbon-cycle dynamics based on CO_2 trapped in ice at Taylor Dome, Antarctica, *Nature*, *398*, 121–126.

Jolly, D., et al. (1998), Biome reconstruction from pollen and plant macrofossil data for Africa and the Arabian peninsula at 0 and 6000 years, *J. Biogeogr.*, *25*, 1007–1027.

Joos, F., and M. Bruno (1998), Long-term variability of the terrestrial and oceanic carbon sinks and the budgets of the carbon isotopes ^{13}C and ^{14}C, *Global Biogeochem. Cycles*, *12*, 277–295.

Joos, F., J. L. Sarmiento, and U. Siegenthaler (1991), Estimates of the effect of Southern Ocean iron fertilization on atmospheric CO_2 concentrations, *Nature*, *349*, 772–774.

Joos, F., M. Bruno, R. Fink, T. F. Stocker, U. Siegenthaler, C. Le Quéré, and J. L. Sarmiento (1996), An efficient and accurate representation of complex oceanic and biospheric models of anthropogenic carbon uptake, *Tellus, Ser. B*, *48*, 397–417.

Joos, F., J. C. Orr, and U. Siegenthaler (1997), Ocean carbon transport in a box-diffusion versus a general circulation model, *J. Geophys. Res.*, *102*, 12,367–12,388.

Joos, F., G.-K. Plattner, T. F. Stocker, O. Marchal, and A. Schmittner (1999), Global warming and marine carbon cycle feedbacks on future atmospheric CO_2, *Science*, *284*, 464–467.

Joos, F., I. C. Prentice, S. Sitch, R. Meyer, G. Hooss, G.-K. Plattner, S. Gerber, and K. Hasselmann (2001), Global warming feedbacks on terrestrial carbon uptake under the Intergovernmental Panel on Climate Change (IPCC) emission scenarios, *Global Biogeochem. Cycles*, *15*, 891–907.

Kaplan, J. O., and I. C. Prentice (2002), The stable carbon isotope composition of the terrestrial biosphere: Modeling at scales from the leaf to the globe, *Global Biogeochem. Cycles*, *16*, 1060, doi:10.1029/2001GB001403.

Kaplan, J. O., I. C. Prentice, W. Knorr, and I. C. Prentice (2002), Modeling the dynamics of terrestrial carbon storage since the Last Glacial Maximum, *Geophys. Res. Lett.*, *29*, 2074, doi:10.1029/2002GL015230.

Keir, R. S. (1988), On the late Pleistocene ocean geochemistry and circulation, *Paleoceanography*, *3*, 413–445.

Kutzbach, J. E., and Z. Liu (1997), Response of the African monsoon to orbital forcing in the early to middle Holocene, *Science*, *278*, 440–443.

Kutzbach, J. E., and F. A. Street-Perrott (1985), Milankovitch forcing fluctuations in the level of tropical lakes from 18 to 0 kyr BP, *Nature*, *317*, 130–134.

Leemans, R., and W. P. Cramer (1991), The IIASA climate database for land areas on a grid with 0.5° resolution, *Res. Rep. RR-91-18*, Int. Inst. for Appl. Syst. Anal., Laxenburg, Austria.

Liu, Z., E. Brady, and J. Lynch-Stieglitz (2003), Global ocean response to orbital forcing in the Holocene, *Paleoceanography*, *18*, 1041, doi:10.1029/2002PA000819.

Lloyd, J., and G. D. Farquhar (1994), ^{13}C discrimination during CO_2 assimilation by the terrestrial biosphere, *Oecologia*, *99*, 201–215.

Maslin, M. A., and E. Thomas (2003), Balancing the deglacial global carbon budget: The hydrate factor, *Quat. Sci. Rev.*, *22*, 1729–1736.

Matsumoto, K., J. L. Sarmiento, and M. A. Brzezinski (2002), Silic acid leakage from the Southern Ocean: A possible explanation for glacial atmospheric pCO_2, *Global Biogeochem. Cycles*, *16*, 1031, doi:10.1029/2001GB001442.

Matthews, E. (1983), Global vegetation and landuse: New high resolution data bases for climate studies, *J. Clim. Appl. Meteorol.*, *22*, 237–246.

McGuire, A. D., et al. (2001), Carbon balance of the terrestrial biosphere in the twentieth century: Analyses of CO_2, climate and land use effects with four process-base ecosystem models, *Global Biogeochem. Cycles*, *15*, 183–206.

Monnin, E., A. Indermühle, A. Dällenbach, J. Flückiger, B. Stauffer, T. F. Stocker, D. Raynaud, and J.-M. Barnola (2000), Atmospheric CO_2 concentration over the last glacial termination, *Science*, *291*, 112–114.

New, M., M. Hulme, and P. Jones (2000), Representing twentieth-century space-time climate variability: Development of 1901–95 monthly grids of terrestrial surface climate, *J. Clim.*, *13*, 2217–2238.

Otto, D., D. Rasse, J. Kaplan, P. Warnant, and L. François (2002), Biospheric carbon stocks reconstructed at the Last Glacial Maximum: Comparison between general circulation models using prescribed and computed sea surface temperatures, *Global Planet. Change*, *33*, 117–138.

Otto-Bliesner, B. L., and E. C. Brady (2001), Tropical Pacific variability in the NCAR Climate System Model, *J. Clim.*, *14*, 3587–3607.

Peltier, W. R. (1994), Ice-age paleotopography, *Science*, *265*, 195–201.

Peng, C. H., J. Guiot, and E. Van Campo (1998), Estimating changes in terrestrial vegetation and carbon storage: Using palaeoecological data and models, *Quat. Sci. Rev.*, *17*, 719–735.

Pope, V. D., M. L. Gallani, P. R. Rowntree, and R. A. Stratton (2000), The impact of new physical parameterizations in the Hadley Centre climate model: HadAM3, *Clim. Dyn.*, *16*, 123–146.

Prentice, I. C., D. Jolly, and BIOME 6000 Participants (2000), Mid-Holocene and glacial-maximum vegetation geography of the northern continents and Africa, *J. Biogeogr.*, *27*, 507–519.

Prentice, K. C., and I. Y. Fung (1990), The sensitivity of terrestrial carbon storage to climate change, *Nature*, *346*, 48–51.

Ridgwell, A. J., A. J. Watson, M. A. Maslin, and J. O. Kaplan (2003), Implications of coral reef buildup for the controls on atmospheric CO_2 since the Last Glacial Maximum, *Paleoceanography*, *18*, 1083, doi:10.1029/2003PA000893.

Ruddiman, W. F. (2003), The anthropogenic greenhouse era began thousands of years ago, *Clim. Change*, *61*, 261–293.

Scholze, M., J. O. Kaplan, W. Knorr, and M. Heimann (2003), Climate and interannual variability of the atmosphere-biosphere $^{13}CO_2$ flux, *Geophys. Res. Lett.*, *30*, 1097, doi:10.1029/2002GL015631.

Shackleton, N. J. (1977), Carbon-13 in *uvigerina*: Tropical rainforest history and the equatorial Pacific carbonate dissolution cycles, in *The Fate of Fossil Fuel CO_2in the Ocean*, edited by N. R. Andersen and A. Malahoff, pp. 401–428, Plenum, New York.

Shin, S., Z. Liu, B. Otto-Bliesner, E. C. Brady, J. E. Kutzbach, and S. P. Harrison (2002), A simulation of the Last Glacial Maximum climate using the NCAR-CCSM, *Clim. Dyn.*, *20*, doi:10.1007/s00382-002-0260-x, 127–151.

Siegenthaler, U., and F. Joos (1992), Use of a simple model for studying oceanic tracer distributions and the global carbon cycle, *Tellus, Ser. B*, *44*, 186–207.

Sitch, S. (2000), The role of vegetation dynamics in the control of atmospheric CO_2 content, Ph.D. thesis, Lund Univ., Lund, Sweden.

Sitch, S., et al. (2003), Evaluation of ecosystem dynamics, plant geography and terrestrial carbon cycling in the LPJ dynamic global vegetation model, *Global Change Biol.*, *9*, 161–185.

Smith, H. J., H. Fischer, M. Wahlen, D. Mastroianni, and B. Deck (1999), Dual modes of the carbon cycle since the Last Glacial Maximum, *Nature*, *400*, 248–250.

Spero, H. J., J. Bijma, D. W. Lea, and B. E. Bemis (1997), Effect of seawater carbonate concentration on foraminiferal carbon and oxygen isotopes, *Nature*, *390*, 497–500.

Stauffer, B., J. Flückiger, E. Monnin, J. Schwander, J. M. Barnola, and J. Chappellaz (2002), Atmospheric CO_2, CH_4 and N_2O records over the past 60,000 years based on the comparison of different polar ice cores, *Ann. Glaciol.*, *35*, 202–208.

Stuiver, M., P. Reimer, E. Bard, J. Beck, G. Burr, K. Hughen, B. Kromer, G. McCormac, J. van der Plicht, and M. Spurk (1998), Intcal98 radiocarbon age calibration, 24,000-0 cal BP, *Radiocarbon*, *40*, 1041–1083.

Sundquist, E. T. (1990), Long-term aspects of future atmospheric CO_2 and sea level changes, in *Sea-Level Change: Washington National Research Council Studies in Geophysics*, edited by R. Revelle, Natl. Acad. Press, Washington, D. C.

Van Campo, E., J. Guiot, and C. Peng (1993), A data-based re-appraisal of the terrestrial carbon budget at the Last Glacial Maximum, *Global Planet. Change*, *8*, 201–289.

Weiss, R. (1974), Carbon dioxide in water and seawater: The solubility of non-ideal gas, *Mar. Chem.*, *2*, 203–215.

Wright, H., J. Kutzbach, T. Webb III, W. Ruddiman, F. Street-Perrot, and P. Bartlein (Eds.) (1993), *Global Climates Since the Last Glacial Maximum*, Univ. of Minn. Press, Minneapolis.

S. Gerber and F. Joos, Climate and Environmental Physics, Physics Institute, University of Bern, Sidlerstrasse 5, CH-3012 Bern, Switzerland. (gerber@climate.unibe.ch; joos@climate.unibe.ch)

B. L. Otto-Bliesner, National Center for Atmospheric Research, Boulder, CO, USA. (ottobli@ucar.edu)

I. C. Prentice, Department of Earth Sciences, University of Bristol, Wills Memorial Building, Bristol BS8 1RJ, UK. (colin.prentice@bristol.ac.uk)

P. J. Valdes, School of Geographical Sciences, University of Bristol, University Road, Bristol BS8 1SS, UK. (p.j.valdes@bristol.ac.uk)

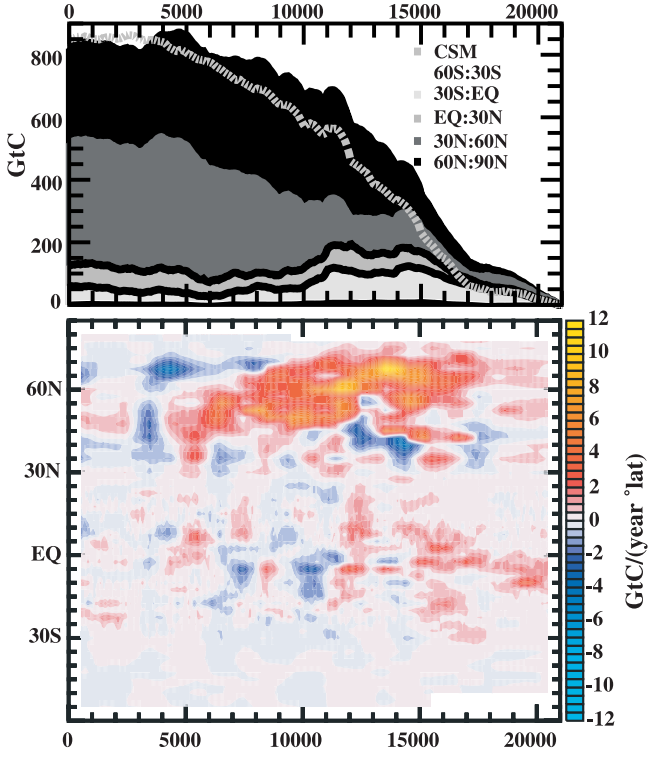

Figure 4. Simulated changes in terrestrial carbon inventory. (top) Cumulative change for different latitude bands for the UM climate anomalies (simulation P1) and global changes for the CSM climate anomalies (dotted line, simulation P1-CSM). The results have been smoothed by a 50-year running mean filter to remove high-frequency variability. (bottom) Zonally integrated net ecosystem uptake (1000-year running means) for the UM climate anomalies (simulation P1).

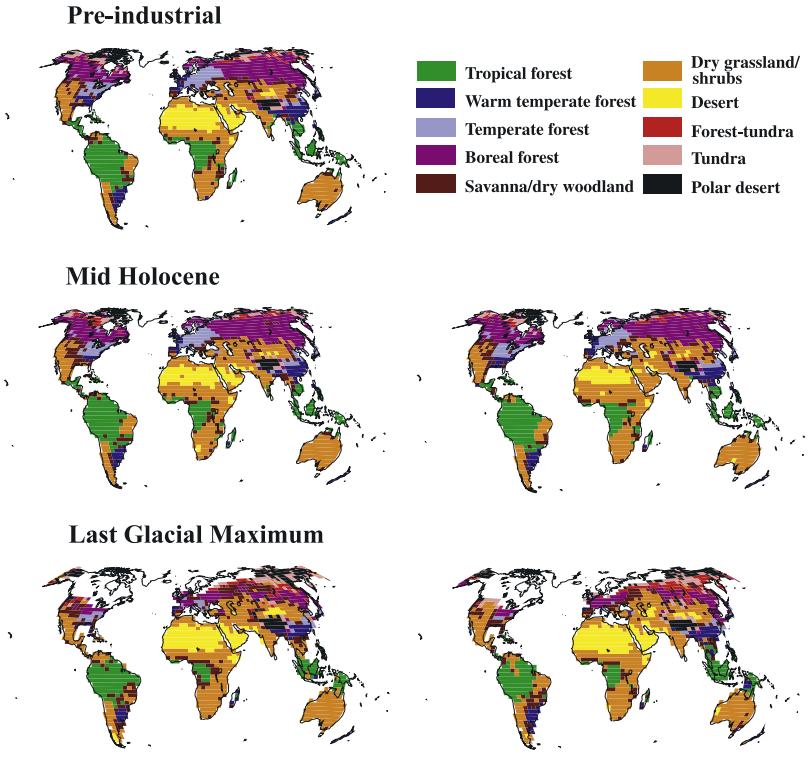

Figure 12. Simulated biome distribution for the LGM (21 ka BP), the Mid-Holocene (6 ka BP), and the pre-industrial time (0 ka) for the UM climate anomalies (left, simulation P1) and the CSM climate anomalies (right, simulation P1-CSM). The distribution at pre-industrial time is nearly identical for simulations with the UM and the CSM anomalies (not shown).